https://doi.org/10.5194/tc-2020-219
Preprint. Discussion started: 19 August 2020

The Cryosphere
Discussions

Atmospheric extremes triggered the biggest calving event in more than 50 years at the Amery Ice shelf in September 2019

Diana Francis [1*], Kyle S. Mattingly [2], Stef Lhermitte [3], Marouane Temimi [1], Petra Heil [4]

[1] Khalifa University of Science and Technology, P. O. Box 54224, Abu Dhabi, United Arab Emirates.

[2] Institute of Earth, Ocean, and Atmospheric Sciences, Rutgers University, New Brunswick, NJ, USA.

[3] Department of Geoscience and Remote Sensing, Delft University of Technology, Mekelweg 5, 2628 CD Delft, Netherlands.

[4] University of Tasmania, Hobart, Tasmania 7001, Australia.

* *Corresponding Author:* diana.francis@ku.ac.ae.

Abstract

Ice shelf instability is one of the main sources of uncertainty in Antarctica's contribution to future sea level rise. Calving events play crucial role in ice shelf weakening but remain unpredictable and their governing processes are still poorly understood. In this study, we analyze the unexpected September 2019 calving event from the Amery Ice Shelf, the largest since 1963 and which occurred almost a decade earlier than expected, to better understand the role of the atmosphere in calving. We find that atmospheric extremes provided a deterministic role in this event. The calving was triggered by the occurrence of a series of anomalously-deep and stationary explosive twin polar cyclones over the Cooperation and Davis Seas which generated strong offshore winds leading to increased sea ice removal, fracture amplification along the pre-existing rift, and ultimately calving of the massive iceberg. The observed record-anomalous atmospheric conditions were promoted by blocking ridges and Antarctic-wide anomalous poleward transport of heat and moisture. Blocking highs helped in (i) directing moist and warm air masses towards the ice shelf and in (ii) maintaining stationary the observed extreme cyclones at the front of the ice shelf for several days. Accumulation of cold air over the ice sheet, due to the blocking highs, led to the formation of an intense cold-high pressure over the ice sheet, which helped fuel sustained anomalously-deep cyclones via increased baroclinicity. Our results stress the importance of atmospheric extremes in ice shelf instability and the need to be accounted for when considering Antarctic ice shelf variability and contribution to sea level, especially given that more of these extremes are predicted under a warmer climate.

https://doi.org/10.5194/tc-2020-219
Preprint. Discussion started: 19 August 2020

The Cryosphere
Discussions

Keywords: Twin polar cyclones, explosive cyclones, blocking highs, ice shelf instability, calving, East Antarctica, Amery Ice Shelf.

1. Introduction

The rapid collapse of several Antarctic ice shelves, observed recently, and the near-instantaneous acceleration of land-ice discharge into the ocean that follows the collapse, demonstrates the sensitivity of the Antarctic cryosphere to recent warming (e.g., Smith et al., 2019; Rignot et al., 2019). However, large uncertainty remains regarding the response of ice shelves to the globally rising temperatures and to the resulting changes in the atmospheric circulation.

On 25 September 2019, the Amery Ice Shelf – the third largest ice shelf in Antarctica – calved iceberg D28 (1,636 km2, 210 m thick), which was the largest calving event since the early 1960s (Fig. 1). The Amery Ice Shelf is a key drainage channel in East Antarctica (Fricker et al., 2002) draining roughly 16% of the East Antarctic Ice Sheet (Galton-Fenzi et al., 2012). It is considered in balance with its surroundings (King et al., 2009; Galton-Fenzi et al., 2012), despite experiencing strong surface melt in summer. However, over the past 20 years, a large system of rifts (a precursor to calving) in the Amery Ice Shelf, known as the Loose Tooth rift system, has been developing (Fricker et al., 2005; Bassis et al., 2008). Recent studies have shown that the propagation rate of the rifts has been decreasing since 2005 due to increasing thickness of melange ice filling in the rifts, and speculated that forward propagation of the west rift might even stop (e.g., Zhao et al., 2013). Satellite images of the Amery Ice Shelf (Fig. 1) show the largest rift extending in the same direction of the ice flow, widening toward the edge of the ice shelf and from this main rift, with radial rifts extending to the west (T1) and east (T2). Earlier studies predicted that the Amery Ice Shelf would not experience a major calve until at least 2025 or later (e.g., Fricker et al., 2002), and the portion that was expected to calve first was T2 i.e., the one to the east of the current calving. This highlights the need for an improved understanding of the underlying processes of calving events and the role of atmospheric forcing in ice shelf weakening; a precursor to rapid and major changes in ice shelf stability.

Indeed, most of the mass loss from the Antarctic Ice Sheet – the largest uncertainty for future sea level projections – takes place at the fronts of ice shelves and glacier tongues, via iceberg calving and surface and basal melt (e.g., Pritchard et al., 2012; Shepherd et al., 2018). Compared to melting, rifting and subsequent calving is the fastest way by which marine-terminating glaciers lose mass to the ocean and contribute therefore to sea level rise (e.g., Smith et al., 2019). Despite being floating ice (i.e., changes in their mass due to calving do not have a direct contribution to sea level rise), ice shelves act to buttress inland ice by blocking the flow of ice from the interior. This restrictive force decreases when ice shelves thin or calve. Calving from floating ice shelves contributes indirectly to sea-level rise as these events accelerate the rate of ice flow from grounded ice-sheet into the ocean (e.g., Hogg and Gudmundsson, 2017). For example, on the Antarctic Peninsula, such events have been shown to increase by eight-fold the rate of ice flow inland (Rignot et al., 2004; Scambos et al., 2004). This leads to more ice discharge into the oceans and a consequent increase in the ice-sheet contribution to global sea-level rise (Hogg and Gudmundsson, 2017). Ocean-driven thinning was also detected at key ice shelves of the East Antarctic Ice Sheet including the Amery Ice Shelf (Greenbaum et al., 2015; Smith et al., 2019) suggesting that this

https://doi.org/10.5194/tc-2020-219
Preprint. Discussion started: 19 August 2020

region is also susceptible to rapid and large-scale ice loss (Aitken et al., 2016), and could contribute to future sea-level rise (DeConto et al., 2016; Rignot et al., 2019). Therefore, there is an urgent need to assess the sensitivity of East Antarctic ice shelves to atmospheric forcing and to understand the governing processes.

Beyond being part of a natural glaciological process, calving events at Antarctic ice shelves have been attracting much attention recently (e.g., Liu et al., 2015; Benn and Astrom 2018) as they were found to trigger, in some cases, the total disintegration of the parent ice shelf (Cook and Vaughan 2010; Liu et al., 2015; Jeong et al., 2016; Bassis and Ma, 2016; Massom et al., 2018). These events have been attributed mainly to an enhanced regional warming (Vaughan et al., 2012; Pitchard et al. 2012) which increases surface and basal melt as well as to ocean forcing involving intense crevassing and rifting along multiple lines of weakness such as radial crevasses (Liu et al., 2015; Jeong et al., 2016; Bassis and Ma, 2016), and to regional loss of pack ice in the shelf-front area which allows storm-generated ocean swell to flex the outer margins of the shelves and lead to their calving (Massom et al., 2018). However, atmospheric-dynamics forcing during such events, particularly the wind mechanical action on rift widening both directly and via wind-induced waves, remains unexplored.

Despite the importance and the implications of ice shelf calving, this phenomenon remains unpredictable and is still poorly understood. Moreover, the underlying mechanisms governing Antarctic ice shelf instability, especially those associated with atmospheric extremes, remains unknown.

Of particular importance is the impact on Antarctic ice shelves of the poleward shift of extratropical storm tracks (Tamarin and Kaspi, 2017) and the observed increase in the number and intensity of cyclones around Antarctica over the last few decades (Wei and Qin 2016). The poleward shift of extratropical cyclones was found in reanalysis data of recent years (Fyfe, 2003; Son et al., 2008), and models project an estimated poleward shift of cyclone genesis 1° to 2° in latitude on average under enhanced greenhouse gas concentrations (Bengtsson et al., 2009; Barnes and Polvani, 2013). Importantly, this poleward shift was found to be particularly pronounced in the Southern Hemisphere (Chang et al., 2012), and the mean intensity of cyclones as well as the number of extreme cyclones are projected to increase under a warmer climate scenario (Lambert and Fyfe, 2006; Chang, 2017; Kossin et al., 2020).

Changes in cyclone tracks, numbers, and intensity may have significant impacts on Antarctic sea ice and land ice. In fact, weather systems (i.e., cyclones and blocks) resulting from the larger-scale circulation (e.g., Pope et al., 2017) are identified as the main driver of the observed trends in sea ice variability (Matear et al., 2015; Schemm, 2018; Turner et al., 2017; Eayrs et al., 2019). Furthermore, cyclones and their associated atmospheric rivers can induce sea ice melt (Francis et al., 2020), ice-shelf surface melt (Wille et al., 2019) and significant sea ice drift (Kwok et al., 2017; Francis et al., 2019) by virtue of their anomalous moisture and heat transport to high latitudes (Woods & Caballero, 2016; Grieger et al., 2018) and the strong surface winds they carry (Schemm, 2018). Severe storms can generate energetic waves (up to 8 m) in the Southern Ocean capable of penetrating hundreds of kilometers into the sea ice covered ocean (Kohout et al., 2014; Vichi et al., 2019). Concomitantly, the sea ice cover acts as a buffer and attenuates the wave energy over

https://doi.org/10.5194/tc-2020-219
Preprint. Discussion started: 19 August 2020

distance, reducing therefore the impact of storms on ice shelves (Dolatshah et al., 2018; Massom et al., 2018).

An extreme situation in cyclogenesis is the formation of explosive cyclones. These are developing cyclones for which the central pressure decreases by at least 24 hPa in 24 hours (Sanders and Gyakum, 1980). Explosively developing cyclones are deeper and longer-lasting compared to ordinary cyclones and they are found to be more intense in the Southern Hemisphere than in the Northern Hemisphere (Raele et al., 2019). In particular, explosive cyclones in the Indian Ocean sector of the Southern Ocean (close to South Africa) are stronger and express higher deepening rates than elsewhere around Antarctica (Raele et al., 2019). This same region (between 45°E and 90°E and poleward of 40°S) – encompassing the Amery Basin – stands out in a climatological study (Allen et al., 2010) as one of three main regions for explosive cyclogenesis around Antarctica, where explosive cyclones are characterized by a 20hPa mean pressure depth relative to the surrounding pressure field. A climatological study of explosive cyclones (Lim and Simmonds, 2002) found that the number of explosive cyclones increased in both hemispheres during 1979-1999, and that positive trends of such systems are statistically significant in the Southern Hemisphere. On average, the study identified 26 explosive cyclones per year in the Southern Hemisphere and found that explosive cyclones exhibit greater mean intensity and depth relative to the entire population of ordinary cyclonic systems. A more recent climatological study over a longer period (1979–2013) reported similar findings, with an increase in the frequency of explosive cyclones in the band of 45°–55°S during winter and early spring (Wei and Qin 2016).

The spatial distribution of these cyclones was found to have a close association with that of strong baroclinicity. In general, the preferred region for cyclogenesis is where both a strong temperature gradient and an upper-level trough are present (e.g., Shimada et al., 2014). While high baroclinic instability associated with the horizontal temperature gradient is crucial for the formation and the intensification of cyclones (Davies, 1997, Uccellini, 1990), cyclogenesis occurs only at the entrance and exit regions of upper-level troughs (e.g., Shimada et al., 2014). Around Antarctica, the strongest temperature gradient is found during late winter-early spring along the fringes of the ice pack, making the sea-ice edge a preferred region for cyclogenesis (e.g., Schlosser et al., 2011; Stoll et al., 2018). However, the location of the temperature gradient relative to the ice edge depends strongly on the atmospheric circulation at larger scale, where a strong temperature gradient can occur poleward of the ice edge (i.e., closer to the ice shelves) during an enhanced zonal wave number three (ZW3) pattern (Francis et al., 2019). This pattern is characterized by the alternation of 3 troughs and 3 ridges around Antarctica. Strong poleward transport of heat and moisture occurs in the ascending branch of troughs and strong equatorward transport of cold air occurs in the descending branch of ridges (e.g., Raphael, 2007). This zonally-alternating pattern of cold and warm air masses creates temperature differences between the different sectors, fuels frontogenesis and promotes the development of explosive cyclones close to the ice shelves and over the sea ice cover.

Another aspect of the ZW3 pattern is the impact of the ridges on the propagation speed of the cyclones. In the troughs, the extratropical cyclones and the associated moisture and heat fluxes are directed poleward; once they reach the Antarctic coast they are blocked by the ridges to their east

https://doi.org/10.5194/tc-2020-219
Preprint. Discussion started: 19 August 2020

(Francis et al., 2019; 2020). This results in stationary cyclones over the same region for 1-2 days which in turn induces pronounced impact on the sea ice (e.g., Francis et al., 2019) and waves (Vichi et al., 2019). The same scenario can happen at the front of ice shelves during winter-spring if the cyclones form closer to the coast and/or the sea ice extent decreases under a warmer climate. Interestingly, the Antarctic sea ice extent has been decreasing since 2015 (Swart et al., 2018) and the ZW3 index has been the most positive on record during the same period (Schlosser et al., 2018; Francis et al., 2019). Increased warm air advection toward Antarctica was found to be at the origin of the observed negative anomaly in Antarctic sea ice extent in recent years (Schlosser et al., 2018). Given the dual impact of ZW3 circulation on both explosive cyclogenesis (location and intensity) and sea ice extent, this combination may result in a more pronounced impact of extreme cyclones on ice shelves.

Another extreme situation in cyclogenesis is the formation of twin cyclones during which the resulting effect of the mutually-interacting cyclones is twice as strong as the individual cyclones (e.g., Moustaoui et al., 2002). To our knowledge, the formation of explosively developing twin cyclones has been, to date, only observed and studied in the tropics (Ferreira et al., 1996; Moustaoui et al., 2002), in the mid-latitudes (Yokoyama and Yamamoto, 2019) and in the Arctic (Renfrew et al., 1997). In this study, we report for the time, the formation of polar twin cyclones near Antarctica during two consecutive events; one on 19-20 September 2019 at 60°E and the second on 23-24 September 2019 at 85°E.

Despite the observed poleward shift of extratropical cyclones, the increasing number and intensity of explosive cyclones around Antarctica and the decline in sea ice extent in recent years, the impact of extreme cyclones on ice shelves instability has not been investigated to date. This is the objective of this study.

Building on previous studies that investigated these patterns separately, we aim in this study to assess the impact of extreme cyclone activity during the largest calving event since 1963 at the Amery Ice Shelf. Using satellite data and atmospheric reanalyses, we investigate the role of atmospheric forcings in this calving event which occurred under a ZW3-like situation. The development of the explosive cyclones and their impact on sea ice and land ice conditions are addressed in section 2. Section 3 discusses our findings. The data and methods used in this study are described in section 4.

https://doi.org/10.5194/tc-2020-219
Preprint. Discussion started: 19 August 2020

The Cryosphere
Discussions
Open Access

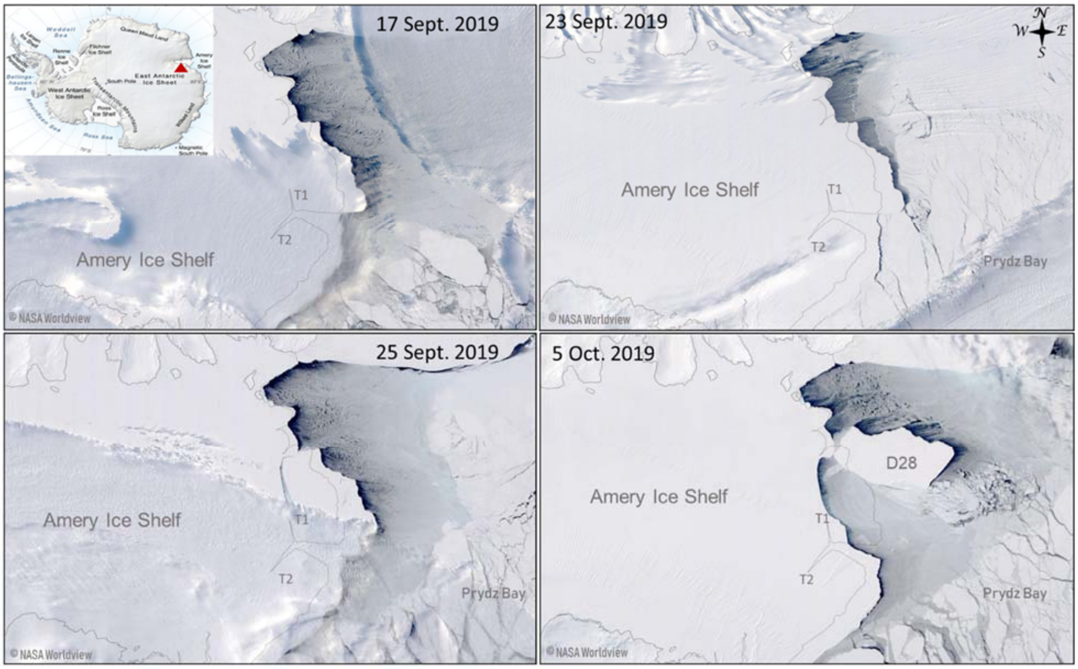

Figure 1: MODIS satellite visible imagery of the Amery Ice Shelf and the Loose Tooth rift system (T1 and T2) at its front. Ice conditions are shown before the calving on 17 and 23 September 2019, during the calving on 25 September 2019, and few days after the detachment of the new iceberg D28. Image credit NASA Worldview.

2. Results

2.1 Explosive twin cyclones during 18-22 September 2019 – preconditioning

In September 2019, the synoptic conditions exhibited an amplified zonal wave number 3 (ZW3) pattern characterized by 3 trough/ridge systems associated with low/high mean sea level pressure (MSLP) anomalies. Compared to all Septembers in the 1979-2019 period, the broad scale MSLP anomaly indicates that, for September 2019, there was below average pressure over much of the Antarctic continent and above average pressure to the north (Fig. 2a). In the Indian Ocean sector, the MSLP anomalies exceeded one standard deviation from the mean over large areas with the strongest troughing over Cooperation and Davis Seas (Fig. 2a). To the west of this low pressure anomaly, the South Atlantic ridge exhibited strong positive anomalies exceeding 2 standard deviations from the mean (Fig. 2a). To the east of the low pressure anomaly around the Amery Ice Shelf, another pronounced ridge encompassing south Australia and the Mawson Sea with positive MSLP anomalies exceeded 1 standard deviation from the climatological mean (Fig. 2a).

On a daily scale, the aforementioned synoptic setting was synonym of frequent and extreme weather systems. On 17 September 2019 at 0200 UTC, an extratropical cyclone associated with a 968 hPa low-pressure at its center and located at 60°S, 40°E, started to deepen while moving poleward and eastward. It reached the western side of Cooperation Sea on 18 September 2019 at

https://doi.org/10.5194/tc-2020-219
Preprint. Discussion started: 19 August 2020

The Cryosphere Discussions
Open Access
EGU

0200 UTC with a 940 hPa minimum pressure and remained over this region the entire day (Fig. 2b), then decayed on 19 September 2019 at 1300 UTC. The rapid deepening of the low pressure is characteristic of explosive cyclones (e.g., Sanders and Gyakum, 1980). The explosive cyclone on 18 September 2019 was associated with significant poleward transport of moisture (Fig. 2c) and heat (Fig. 2d) carried by an atmospheric river propagating poleward adjacent to the low-pressure center. The atmospheric river was associated with integrated water vapor transport (IVT) greater than 500 kg m^{-1} s^{-1} at its core, with IVT values around 100 kg m^{-1} s^{-1} over Prydz Bay exceeding the 99th percentile of September climatology in this region (Fig. 3a).

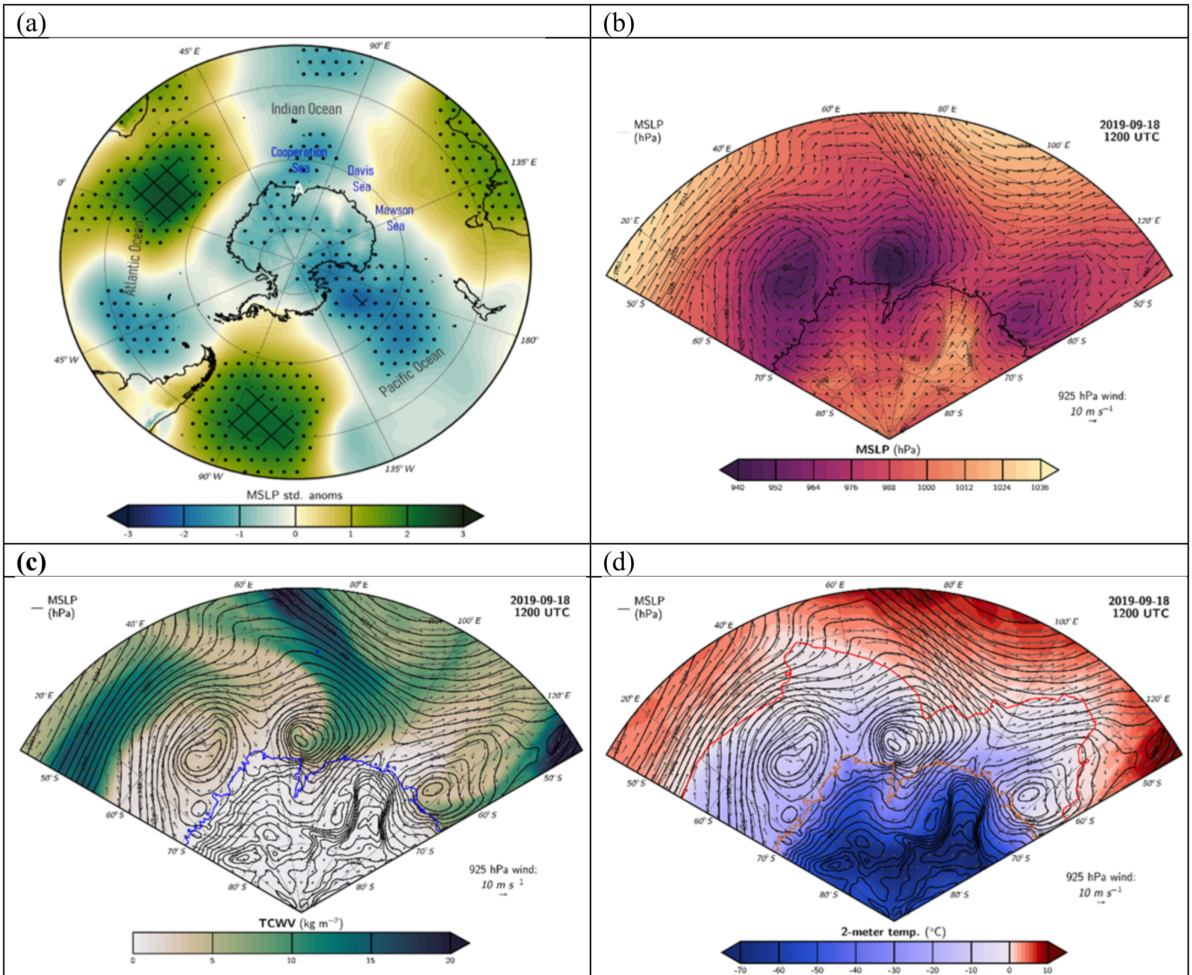

Figure 2: Normalized anomalies of Mean Sea Level Pressure (MSLP) for September 2019 relative to the 1979-2019 September climatology. Black dots are regions where the normalized anomalies are larger than 1 standard deviation from the mean and black squares are regions where the normalized anomalies are larger than 2 standard deviations from the mean. The letter A in white indicates the location of the Amery Ice Shelf. (b) MSLP (shaded) and winds at 925hPa (vectors) at 18 September 2019 1200 UTC, (c) same as (b) but for the total column water vapor (TCWV) in colors, winds at 925hPa in vectors and MSLP in

https://doi.org/10.5194/tc-2020-219
Preprint. Discussion started: 19 August 2020

The Cryosphere Discussions
Open Access

black contours, (d) same as (c) but for 2-m temperature (in colors), winds at 925hPa in vectors, MSLP in black contours and 0°C contour in red.

In the Southern Hemisphere, where cyclonic winds spin clockwise, the highest wind speed occurs along the bent-back front of the cyclone, i.e., to the left of the low-pressure center of the cyclone (e.g., Wagner et al., 2011, Watanabe and Niino, 2014). This was observed during the explosive cyclone on 18 September 2019 which generated extremely strong surface winds to the left of its center exceeding 20 m s^{-1} (Fig. 3b). Being stationary over Cooperation Sea but to the west of the Amery Basin, this extreme cyclone generated a sustained northeasterly wind stress over the northern part of the ice shelf (Fig. 3b), as well as strong poleward warm and moist air advection (Fig. 2c, 2d and 3a). The combination of warm temperatures brought by the cyclone/AR and strong easterly/northeasterly wind speeds was unusual (Fig. 3). MSLP anomalies during this event were in excess of -4 sigma (Fig. 3b), with MSLP values below the 1st percentile of September climatology over a large area along and to the north of the ice shelf margin (Fig. 3b). Extreme wind anomalies exceeding the 99th percentile over the central and eastern ice shelf margin were associated with this cyclone from 18 September through 19 September 2019 (Fig. 3c). Likewise, there were sustained positive 2-m temperature anomalies throughout the period exceeding 2 standard deviations from the climatological mean (Fig. 3d).

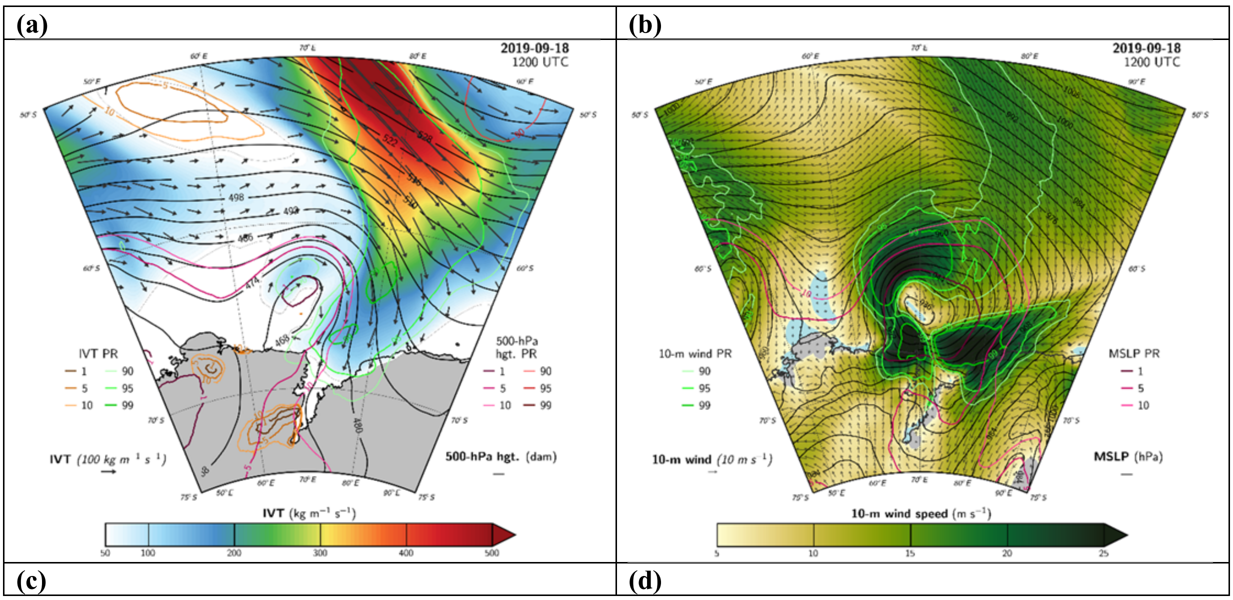

https://doi.org/10.5194/tc-2020-219
Preprint. Discussion started: 19 August 2020

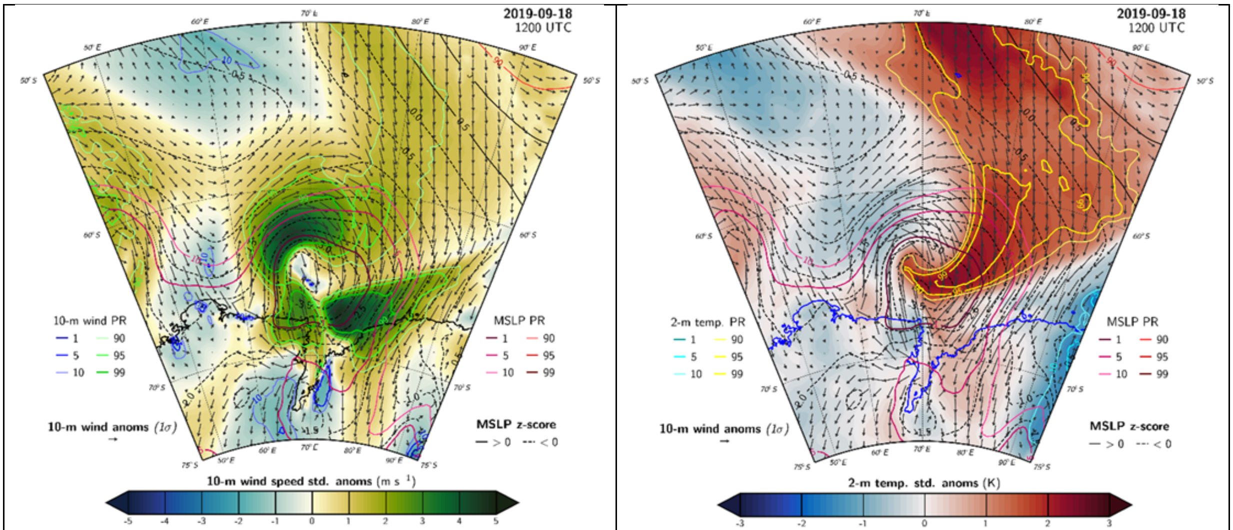

Figure 3: Maps on 18 September 2019 at 1200 UTC of (a) Integrated water vapor transport (IVT) shaded, geopotential heights at 500 hPa in black contours and IVT direction in black vectors, (b) 10-m wind speed in colors, 10-m wind direction in black vectors and MSLP in black contours. (c) Standardized 10-m wind speed anomalies relative to the full September record (1979-2019) (d) Same as (c) but for 2-m temperature. Colored contour lines show percentile rank extremes (1, 5, 10 and 90, 95, 99 percentile ranks) of the corresponding quantities indicated on the plots. On (c) and (d): Vectors show 10-m wind anomalies, black contours show positive MSLP anomalies and dashed black contours show negative MSLP anomalies.

The first explosive cyclone on 18 September 2019 was followed immediately by a second explosive cyclone which approached Cooperation Sea from the west on 19 September at 1400 UTC with a deep low of 952hPa. At 2000UTC, this deep cyclone widened and evolved into two twin polar cyclones over the same region (Fig. 4a). The twin cyclones exhibited 960hPa low-pressure at their respective centers and remained active to the west of the Amery Ice Shelf for three consecutive days (Fig. 4a). Their signatures dissipated in the pressure field on 22 September 2019 at 0000UTC. The poleward transport of heat (Fig. 4b) and moisture (Fig. 4c) towards the Amery Ice Shelf continued during this event together with extreme wind stress exceeding the 99th percentile (Fig. 4d). Being stationary to the west of the Amery Ice Shelf (Fig. 4a), the twin cyclones induced extreme easterly winds across the ice shelf, with u-wind anomalies exceeding -5 sigma of September climatology over the western ice shelf from 19 September 2019 at 1900 UTC through 20 September at 1100 UTC (Fig. 4d) and below the 1 percentile u-wind values over the whole lower ice shelf area (Fig. 4d). When compared with the climatology for all months during 1979-2019, many hourly wind speeds over the ice shelf front during 18-20 September were substantially greater than the 99th percentile of climatology, with the most anomalous wind speeds on 18 September (Fig. 6e).

On 21 September 2019, the twin cyclones merged and moved to the area in front of the Amery Ice Shelf (Fig. 4e) resulting in a deep cyclone associated with MSLP at its center below the 5th percentile. The remnant cyclone slowly meandered along the northern margin of Prydz Bay and

https://doi.org/10.5194/tc-2020-219
Preprint. Discussion started: 19 August 2020

The Cryosphere
Discussions
Open Access
EGU

decayed on 22 September 2019. Anomalously warm air masses were brought by this cyclone over the margins of the Amery Ice Shelf exceeding the 90th percentile (Fig. 4e). MODIS satellite imagery on this day showed a swirling cyclone at the mouth of the Amery Ice Shelf (Fig. 4f). Sentinel-3A and 3B observations on 22 September 2019 at 0000 UTC (i.e., during the decay of the cyclones) show elevated waves at the ice-shelf front area reaching 6 m significant wave height (Fig. 4g). Waves generated by the cyclones during the 18-21 September 2019 period, when easterly wind speeds were stronger, may have been substantially higher. The easterly direction of the winds during this episode infers that the wind-induced wave at the ice shelf front occurred likely in a direction parallel to the pre-existing rift T1 at the western side of the front.

Surface melt during this event may have occurred briefly due to the anomalous warm and moist air masses. However, the inspection of daily satellite images of Sentinel-1 backscatter coefficient, MODIS ice surface temperature and AMSR2 brightness temperature did not show any prolonged nor significant surface melt at the Amery Ice Shelf during this event.

In summary, an extended period of strong cyclonic activity from 18-22 September 2019 resulted in exceptional period of strong easterly / northeasterly winds over the western side of the Amery Ice Shelf where the climatology shows a positive zonal component. This exceptional wind stress on the ice shelf generated strong waves in the region in front of the ice shelf. The advection of anomalous warm and moist air masses to the area at the ice shelf front may have contributed to a decrease in sea ice concentration at the front of the ice shelf, as it will be shown in section 5.

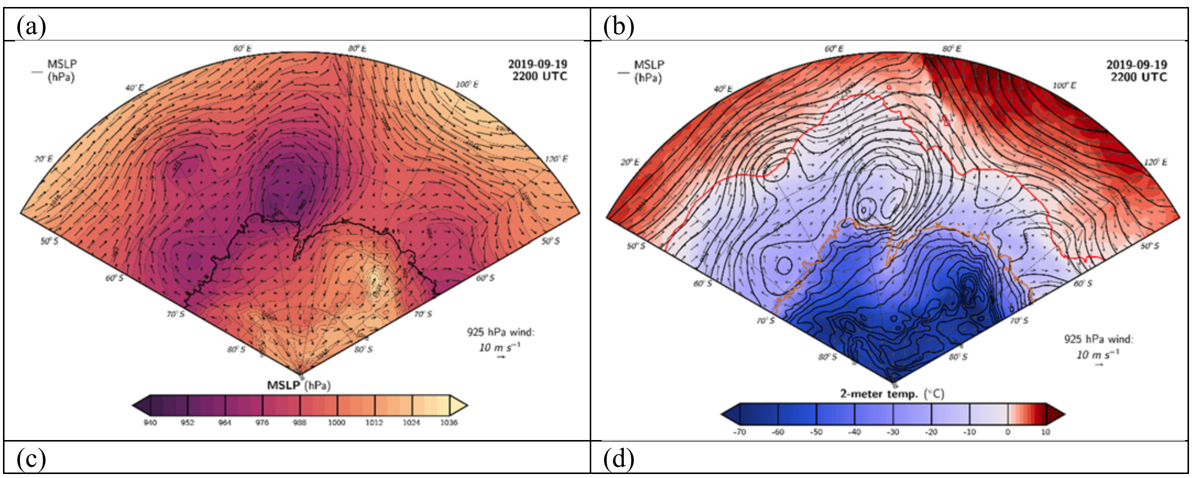

https://doi.org/10.5194/tc-2020-219
Preprint. Discussion started: 19 August 2020

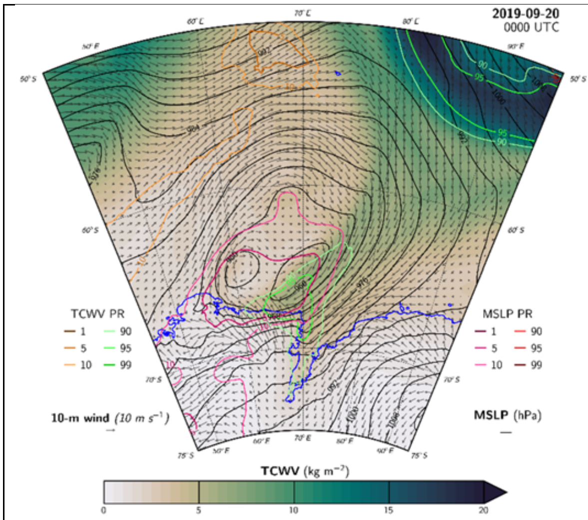

(e)

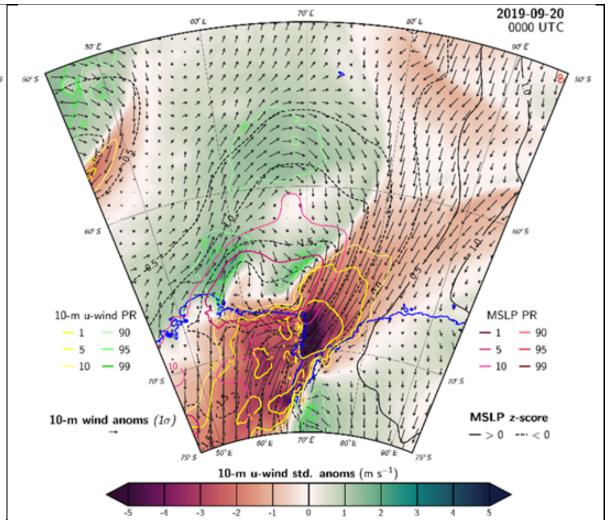

(f)

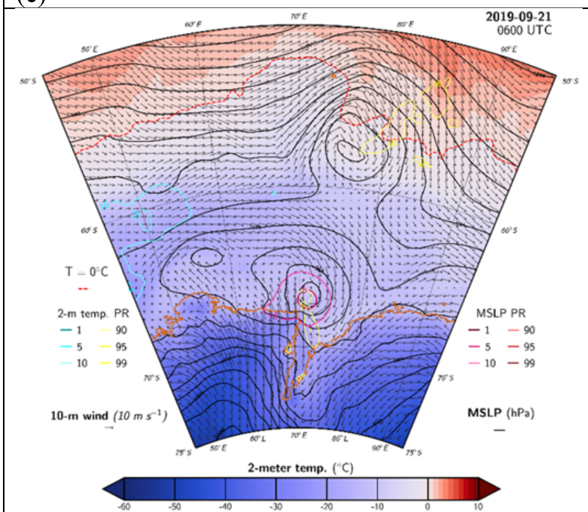

(g)

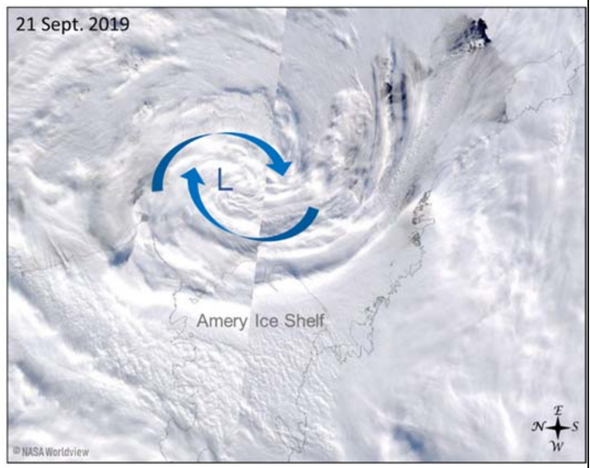

https://doi.org/10.5194/tc-2020-219
Preprint. Discussion started: 19 August 2020

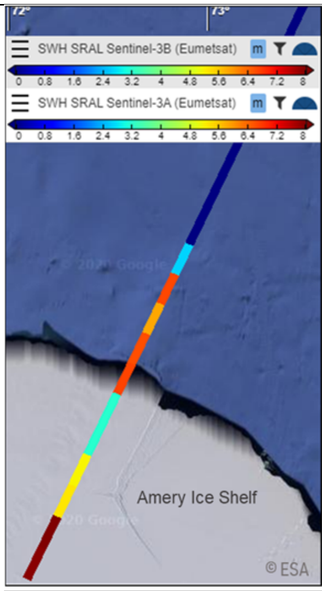

Figure 4: ERA5 reanalysis of: (a) MSLP in colors and winds at 925hPa in vectors on 19 September 2019 at 2200 UTC, (b) 2-m temperature in colors, winds at 925hPa in vectors, MSLP in black contours and 0°C contour in red on 19 September at 2200 UTC, (c) total column water vapor (TCWV) in colors, winds at 925hPa in vectors and MSLP in black contours on 20 September 2019 at 0000 UTC, (d) standardized anomalies relative to the full record (1979-2019) of 10-m u-wind on 20 September 2019 at 0000 UTC. Vectors show 10-m wind anomalies, black contours show positive MSLP anomalies and dashed black contours show negative MSLP anomalies. Colored contour lines show percentile rank extremes (1, 5, 10 and 90, 95, 99 percentile ranks) of the corresponding quantities indicated on the plots, (e) 2-m temperature in colors, 10-m winds in vectors, MSLP in black contours and 0°C contour in red dashed-line on 21 September at 0600 UTC. (f) MODIS visible imagery on 21 September 2019, image credit: NASA worldview. (g) Sentinel-3A and 3B observations of wave height on 22 September 2019 at 0000 UTC, image credit: ESA Ocean Virtual Laboratory.

2.2. Twin polar cyclones during 23-24 September 2019 - calving

Following the extended period of extreme cyclones in Cooperation sea, an explosive cyclone started to develop on 21 September 2019 centered at 45°E and 60°S. The pressure at its center deepened from 976hPa on 21 September at 1900 UTC to 952hPa on 22 September 2019 at 19 UTC (not shown). On 23 September 2019, the large explosive cyclone entered Cooperation Sea from the west with a deep low of 940 hPa (Fig. 5a). It was accompanied by an intense atmospheric river exhibiting core IVT greater than 800 kg m^{-1} s^{-1} and stretching from mid-latitudes towards Antarctica (Fig. 5b). The explosive cyclone was stationary over Cooperation Sea during the whole day on 23 September 2019, being trapped between two far-south reaching blocking ridges one to the west of it and the second to its east (Fig. 5a and 5c). The cyclone intensified, increased in size and evolved into twin cyclones on 24 September 2019 at 0000 UTC associated with 952hPa low pressure at their respective centers (Fig. 5c and 5d). The mutual interaction between the two cyclones appeared as co-rotation and an eastward translation of the binary pair by the ambient

https://doi.org/10.5194/tc-2020-219
Preprint. Discussion started: 19 August 2020

flow. The interplay between the cyclones lasted for one day after which the twins merged and decayed on 25 September 2019.

To the south of the twin cyclones, a cold pressure high (1036 hPa) developed over the ice sheet as a result of the accumulation of cold air due the blocking ridge to the northeast (Fig. 5c). The high-pressure advected extremely cold air masses (2-m temperature below -40°C) into the twin-cyclone system (Fig. 5e and 5 f) which may have fostered baroclinicity and frontogenesis, hence sustaining the twin cyclones for a longer period of time.

Transport of moisture from mid-latitudes toward East Antarctica continued during this period and high precipitable water amounts were continuously advected by the atmospheric river and the cyclones over the ice shelf margins (Fig. 5d). Sustained advection of exceptionally warm air masses was observed during this event as well (Fig. 5e and 5f). Air masses characterized by 0°C 2-m temperatures were seen to penetrate further south reaching 66°S over the region to the east of the twin cyclones during the whole day on 24 September 2019 (Fig. 5e and 5f).

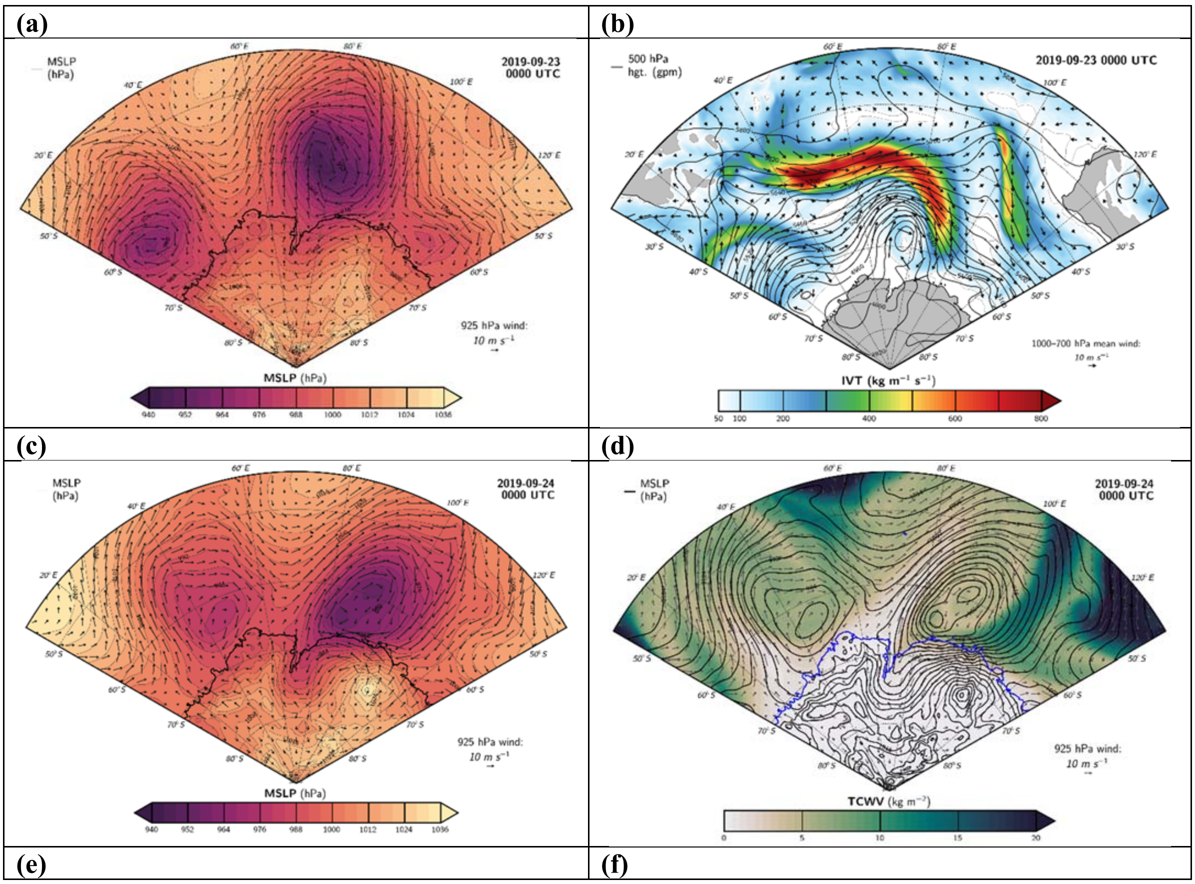

https://doi.org/10.5194/tc-2020-219
Preprint. Discussion started: 19 August 2020

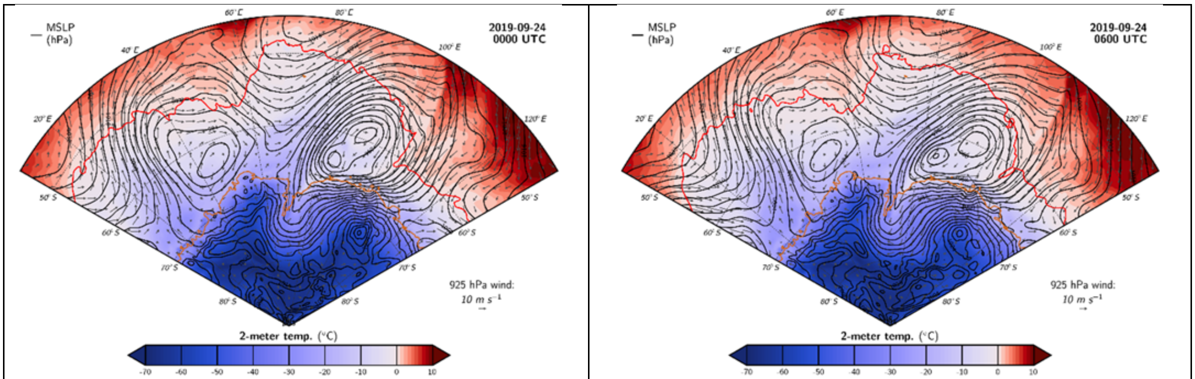

Figure 5: (a) MSLP in colors and winds at 925hPa in vectors on 23 September 2019 at 0000 UTC, (b) integrated water vapor transport (IVT) in colors, geopotential heights at 500 hPa in black contours and 1000-700 hPa mean winds in black vectors on 23 September 2019 at 0000 UTC, (c) total column water vapor (TCWV) in colors, winds at 925hPa in vectors and MSLP in black contours on 24 September 2019 at 0000 UTC, (d) MSLP in colors and winds at 925hPa in vectors on 24 September 2019 at 0000 UTC, (e) 2-m temperature in colors, winds at 925hPa in vectors, MSLP in black contours and 0°C contour in red on 24 September at 0000 UTC, (f) same as (e) but at 0600 UTC.

During 23-24 September, the deep twin polar cyclones were stationary to the east of the Amery Ice Shelf (Fig. 5) associated with MSLP anomalies at their centers below the 5th percentile (Fig. 6a and 6c). They induced extreme westerlies (10-m wind speed in the order of 17 m s^{-1}) across the ice shelf with positive 10-m wind anomalies exceeding 2 standard deviations from the climatological mean (Fig. 6a). The direction of the winds was also exceptional with above 99th percentile u-wind over the western ice shelf margin from 23 September 2019 at 1800 UTC (Fig. 6b) through 24 September 2019 at 1200 UTC and below the 5th percentile u-wind values over the lower eastern ice shelf area (Fig. 6a and 6b). Weaker but still significant (95 percentile) westerly wind anomalies lingered during the remainder of the day on 24 September 2019 and through midday on 25 September 2019 with wind speed at 10-m reaching 15 m s^{-1} at the front of the ice shelf (Fig. 6d). Sustained positive 2-m temperature anomalies were observed throughout the twin cyclone event over the eastern side of Prydz Bay. Warm air advection by the twin cyclones brought 95 percentile rank temperatures over the eastern side of the Amery Ice Shelf and Prydz Bay on 23 and 24 September 2019 and 90 percentile rank temperatures inland over Princess Elizabeth Land (Fig. 6c). These episodes of poleward advection of warm air masses may explain the observed positive-trend in surface temperatures during winter/spring seasons at Prydz Bay reported by Heil (2006) using measurements from ground stations.

The distribution of hourly 10-m wind speed for all months 1979-2019 over the Amery Ice Shelf front is shown in the histogram in Fig. 6f. The winds during the 18-22 September 2019 period were exceptionally unusual compared to the record. The winds during the 23-25 September 2019 period were strong but not unusually extreme. This suggests that the first extreme cyclones' event had an important role in preconditioning the ice shelf front for breakoff, while the offshore winds

https://doi.org/10.5194/tc-2020-219
Preprint. Discussion started: 19 August 2020

during the second event triggered the calving by pushing the iceberg-to-be out from the shelf along the T1 rift.

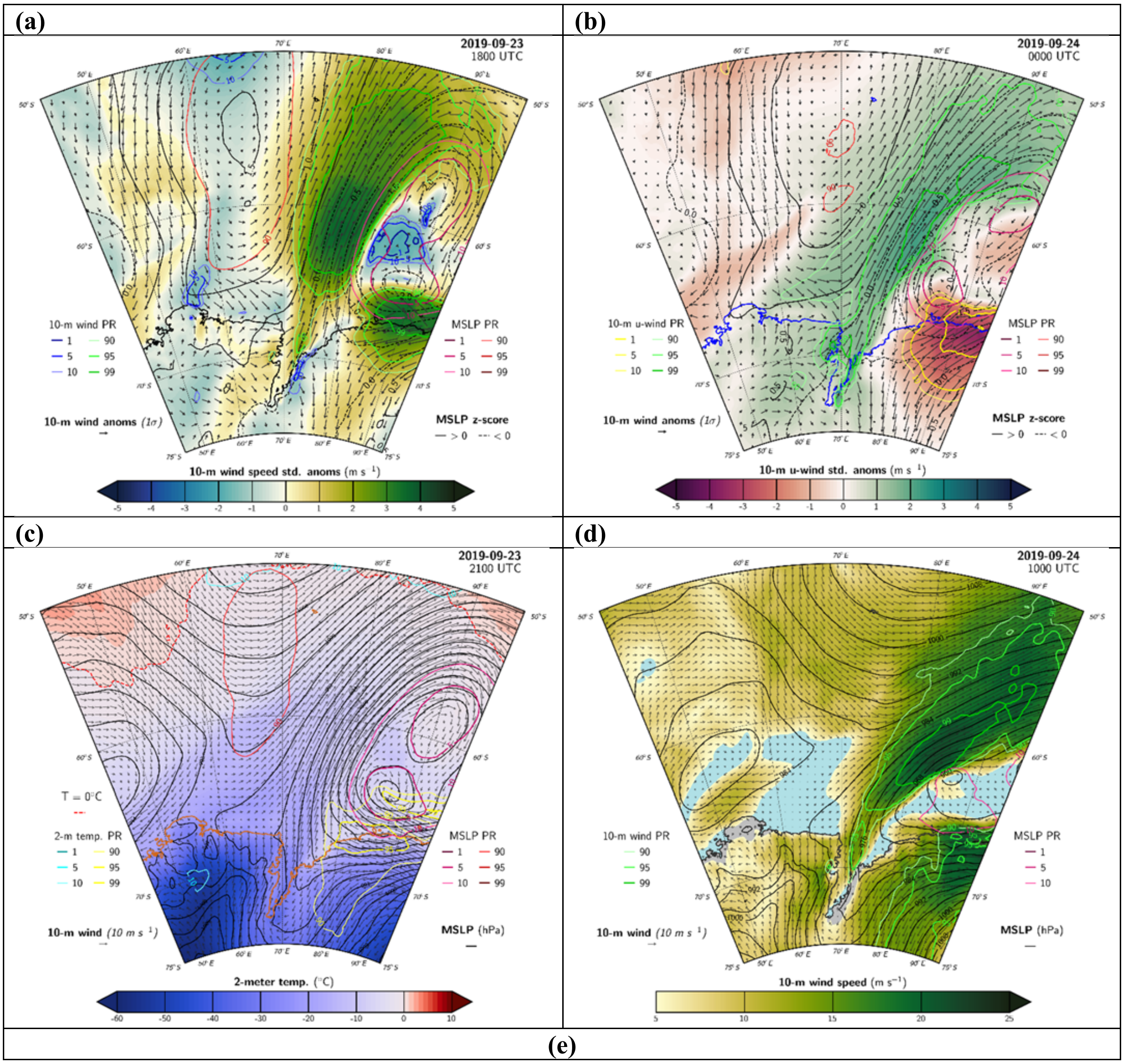

https://doi.org/10.5194/tc-2020-219
Preprint. Discussion started: 19 August 2020

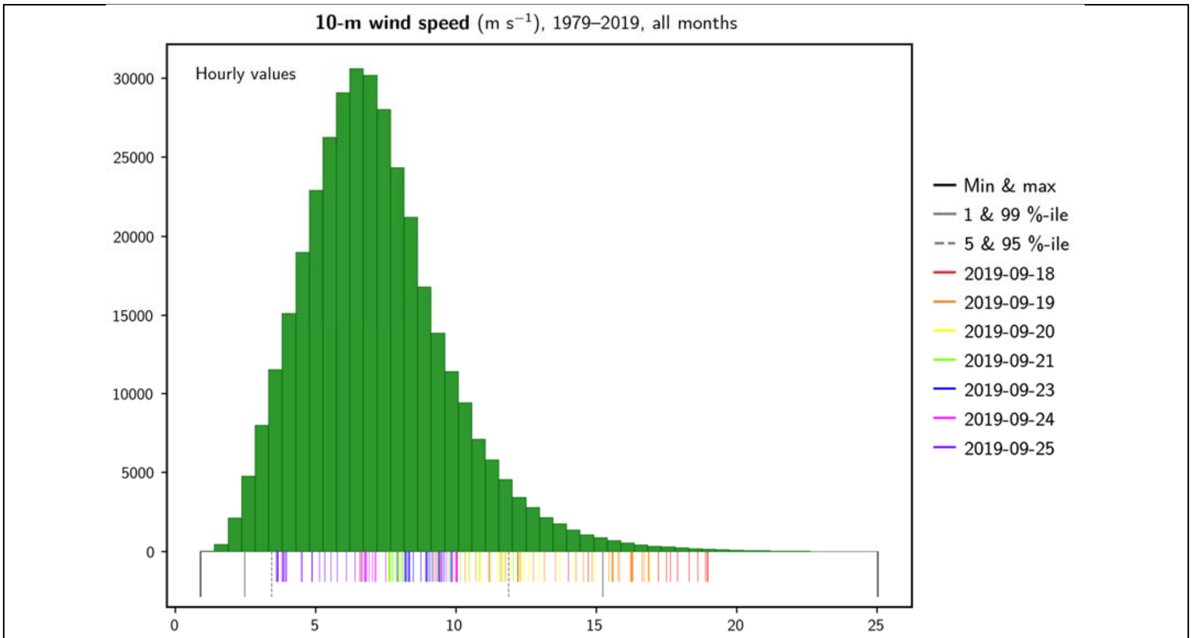

Figure 6: (a) Standardized anomalies relative to the full September record (1979-2019) of 10-m wind speed (colors) at 23 September 2019 1800 UTC. (b) Same as (a) but with u-component of 10-m wind as filled contours at 24 September 2019 0000 UTC. Vectors show 10-m wind anomalies, black contours show positive MSLP anomalies and dashed black contours show negative MSLP anomalies. Colored contour lines show percentile rank extremes (1, 5, 10 and 90, 95, 99 percentile ranks) of the corresponding quantities indicated on the plots. (c) 2-m temperature in colors, winds at 925hPa in vectors, MSLP in black contours and 0°C contour in red dashed-line on 23 September at 2100 UTC. (d) 10-m wind speed in colors, 10-m wind direction in black vectors and MSLP in black contours on 24 September 2019 at 1000 UTC. (e) Histogram showing the distribution of hourly 10-m wind speed for all months during 1979-2019, spatially averaged over 70-65°S and 70-75°E. The colored vertical lines correspond to hourly values during the 18-25 September 2019 period. Each given day in September 2019 has 24 hourly values plotted in the same color.

2.3 Sea ice and land ice conditions

The anomalous atmospheric conditions during the extended period of strong cyclonic activity occurring over the ice cover in Cooperation Sea (i.e., south to the sea ice edge) had significant impacts on both sea ice and land ice (Fig. 7). The sustained period of strong cyclonic activity occurring over the sea ice pack and onto the Amery Ice Shelf caused decreases in sea ice concentration both at the mouth of the Amery Ice Shelf and further offshore. Although this study focuses on the period 17-25 September 2019, the inspection of the sequence of MODIS images for the whole month of September 2019 revealed several episodes of sea ice removal from the ice shelf front area during the 7-17 September 2019 period by offshore winds (i.e., Fig. 1). Despite the formation of new sea ice over the area, the sea ice removal may have preconditioned the sea

https://doi.org/10.5194/tc-2020-219
Preprint. Discussion started: 19 August 2020

The Cryosphere Discussions
Open Access

ice cover for further reduction during the subsequent series of extremes cyclones and increased the area of open water susceptible to ocean wave activity along the front of the ice shelf.

Sea ice concentration in Cooperation Sea and at the Amery Ice Shelf front area was reduced to below 60%, reaching 40% in some places (Fig. 7a and 7b). By the end of the intense cyclonic activity period, areas of open water formed especially at the locations of the strongest surface winds i.e., to the left of the twin cyclones centers (Fig. 7c and 7d). Significant reduction in sea ice concentration was also observed along the sea ice edge associated with wind-driven currents and waves (Fig. 7) which may have decreased the sea-ice attenuation effect of waves-in-ice propagating from lower-latitude ocean toward the ice shelf.

The decrease in sea ice concentration was due to both sea ice melt caused by the anomalous warm and moist air masses advected over the Amery Ice Shelf during the first episode of twin cyclones (i.e., Fig. 3 and 4) and to sea ice drift out of the region by strong winds during the second episode of twin polar cyclones (i.e., Fig. 5 and 6). The strong waves generated locally in the area of reduced sea ice concentration in front of the ice shelf during the first set of cyclone events (Fig. 4g), were important in preconditioning the breakoff by inducing flexure at the front.

Significant sea ice drift was observed at the mouth of the Amery Ice Shelf associated with the exceptional westerlies generated by the twin cyclones on 23-24 September 2019 (Fig. 7e and 7d). The sea ice drift velocity during this period reached 50 km on average per day and the sea ice drifted away from the Amery Ice Shelf towards the east and northeast (Fig. 7f).

(a) **(b)**

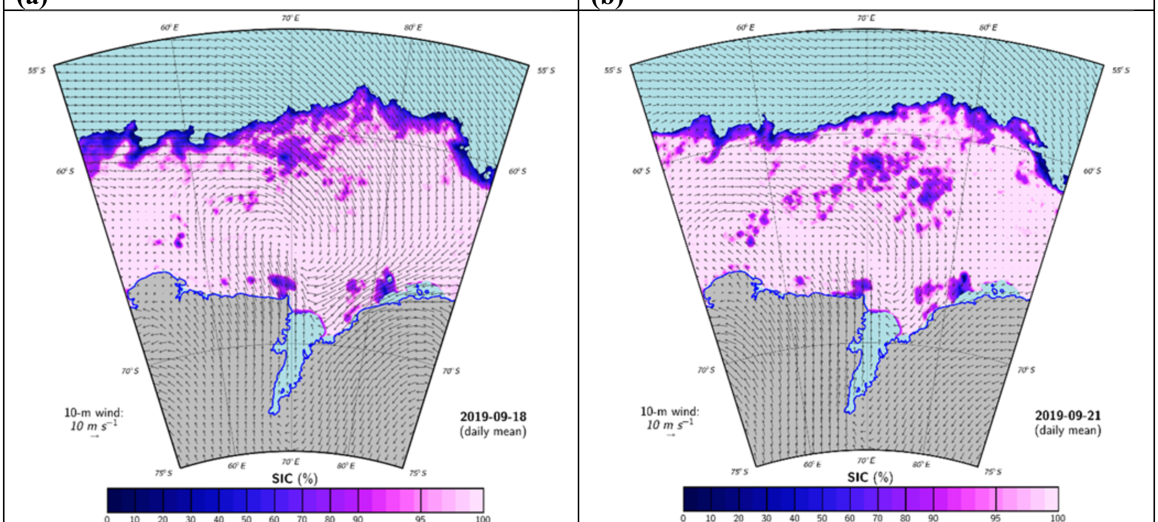

(c) **(d)**

https://doi.org/10.5194/tc-2020-219
Preprint. Discussion started: 19 August 2020

The Cryosphere
Discussions
Open Access

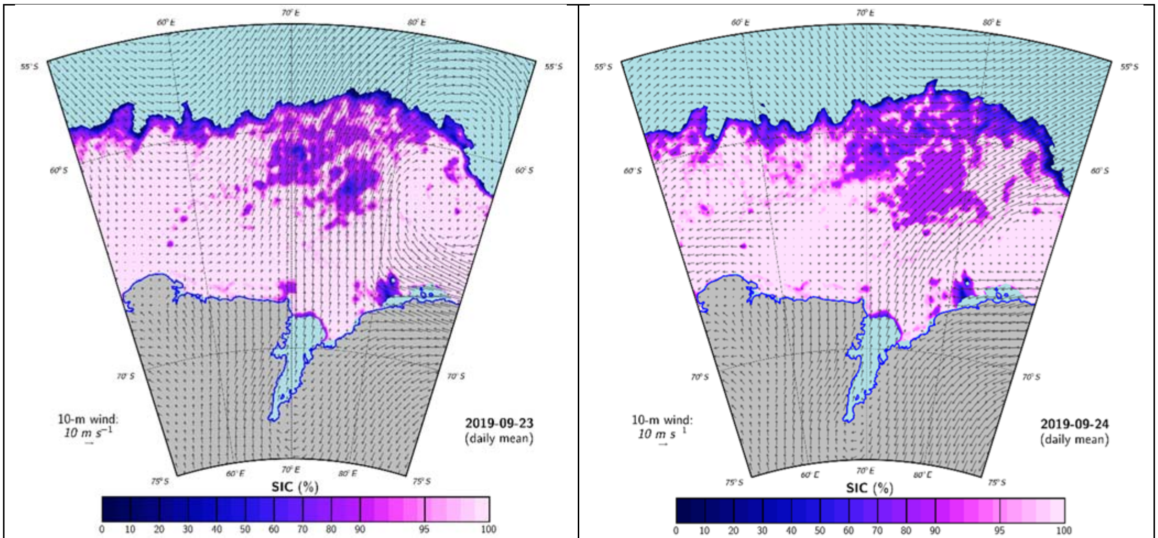

(e) (f)

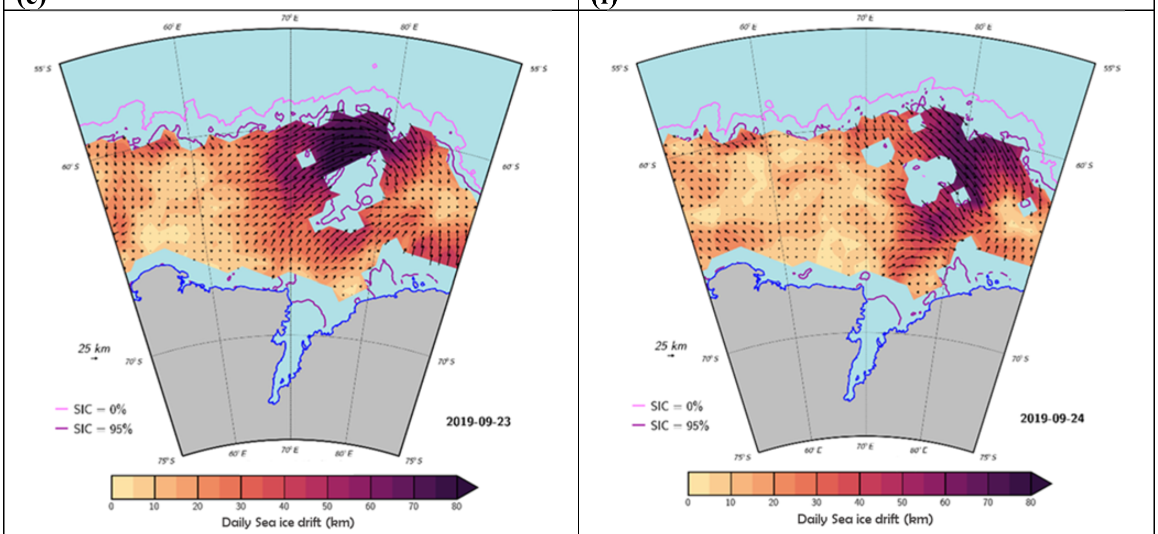

(g)

https://doi.org/10.5194/tc-2020-219
Preprint. Discussion started: 19 August 2020

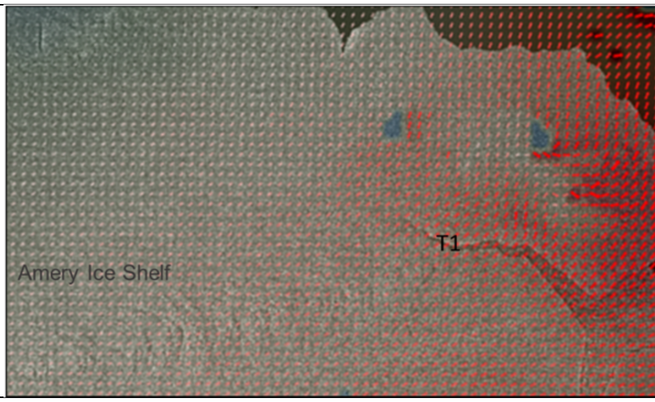

Figure 7: Satellite-derived sea ice concentrations and ERA5-derived daily mean 10-m winds in vectors over 55-75S and 50-90E on: (a) 18 September 2019 at 1200 UTC, (b) on 21 September 2019 at 1200 UTC, (c) 23 September 2019 at 0000 UTC and (d) on 24 September 2019 at 0000 UTC. Satellite-derived daily sea-ice drift velocity in colors and direction in vectors on 23 September 2019 (e) and 24 September 2019 (f). The solid pink contour is the 0% sea ice concentration contour and the solid purple contour is the 95% sea ice concentration contour. (g) SAR image of the Amery Ice Shelf on 23 September 2019. The red vectors correspond to the ice displacement on 23 September 2019 (both velocity and direction) relative to 11 September 2019.

The action of strong winds on sea ice removal from the area at the mouth of the Amery Ice Shelf was visible in MODIS imagery (Fig. 8). During the period of the twin polar cyclones on 23- 24 September 2019, the sea ice was pushed about 65 km away from the ice shelf front in just a 2-day period of time (Fig. 8). The ice-free region in front of the ice shelf presented an asymmetric shape where the sea ice in front of the western side of the ice shelf was pushed further away compared to the sea ice in front of the eastern side (Fig. 8). This may have made the western side more vulnerable to the winds and associated waves induced by the consecutive explosive cyclones.

In fact, sea ice loss in the vicinity of weakened or flooded shelves is considered as the ultimate cause of rapid ice shelf calving (e.g., Massom et al., 2018). The removal of the protective buffer represented by sea ice for ice shelves (e.g., Massom et al., 2018) may have enabled increased flexure of the outer ice shelf western margin by wind-induced waves.

The extreme nature and long duration of the cyclones during the second event induced sustained wind strain on the pre-existing rift at the front of the Amery Ice Shelf, where winds were blowing perpendicular to it. This caused rapid opening of the crack and subsequent movement of the iceberg away from the ice shelf (Fig. 8). The SAR satellite image on 23 September 2019 together with the ice-displacement velocity (rate and direction in vectors) relative to 11 September 2019 are shown in Fig. 7g. The displacement vectors indicate that the iceberg-to-be was rotating in the period 11-23 September 2019 prior to the calving. Wind forcing induced a leftward (relative to the rift T1) splitting-movement of the future iceberg prior to break-off on 25 September 2019.

Explosive cyclones crossing the sea ice zone around Antarctica can generate waves of up to 8 meters in height that are capable of propagating more than 100 km into the sea ice cover (Vichi et

https://doi.org/10.5194/tc-2020-219
Preprint. Discussion started: 19 August 2020

al., 2019). The consecutive deep cyclones under scrutiny impacted immediately the Amery Ice Shelf front since they were found very close to the coast. During the first period of explosive twin cyclones, the cyclones were sitting to the west of the Amery Ice Shelf which directed anomalous warm and moist easterlies towards it. This situation caused a decrease in sea ice concentration (Fig. 7) and intense waves immediately at the shelf front (Fig. 4f) resulting in a cumulative shelf-front fatigue and amplification of the fractures along the pre-existing rifts. This combination of factors weakened the ice shelf front and made it more vulnerable to the additional extreme atmospheric forcing (producing strong offshore winds) and sea ice removal brought by the second event of explosive twin cyclones, ultimately leading to its calving.

Previous studies (Holdsworth and Glynn, 1978; Squire et al., 1994) have shown that calving ice shelves can be triggered by wind-induced waves which impose flexural strains on the ice shelves, with the potential to induce crevasse and rift propagation and calving (Robinson and Haskell, 1992; Bromirski et al., 2010). This effect can be even maximized by the loss of the protective sea ice pack at the front of the ice shelves (Massom et al., 2018). Here we have shown that the series of intense cyclones provided ideal conditions for both sea ice reduction and wind-waves and ultimately triggered the calving on 25 September 2019.

Furthermore, ocean swell (defined as relatively long-period surface-gravity waves that are generated by distant weather systems and are no longer growing or being sustained locally by the wind, as opposed to locally generated wind waves), may have also contributed to (i) fragilizing the western side of the Amery Ice Shelf on 22 September 2019 (i.e., after the decay of the first two twin cyclones) and to (ii) the calving on 25-26 September (i.e., after the decay of the second pair of deep cyclones). Moreover, swells are strongly attenuated by the presence of extensive sea ice which reduced substantially their destructive effect. Thus, loss of sea ice can maximize swell effect on ice shelves. This mechanism has been found at work during the calving events of other Antarctic ice shelves. A study on the calving event in March 1990 at the Erebus Glacier Tongue in the Ross Sea implicated the removal of sea ice combined with ocean swell (Robinson and Haskell, 1990). Focusing on the disintegration of the Larsen ice shelves, Massom et al., (2018) found that regional loss of sea ice before and during the disintegration events allows storm-induced long-period (10–20 s) ocean swells to reach exposed ice shelf fronts that have been preconditioned for calving by extensive fracturing and meltwater flooding. These swells excite flexural oscillations in the outer ice shelf margin which amplify fracture and trigger a calving.

https://doi.org/10.5194/tc-2020-219
Preprint. Discussion started: 19 August 2020

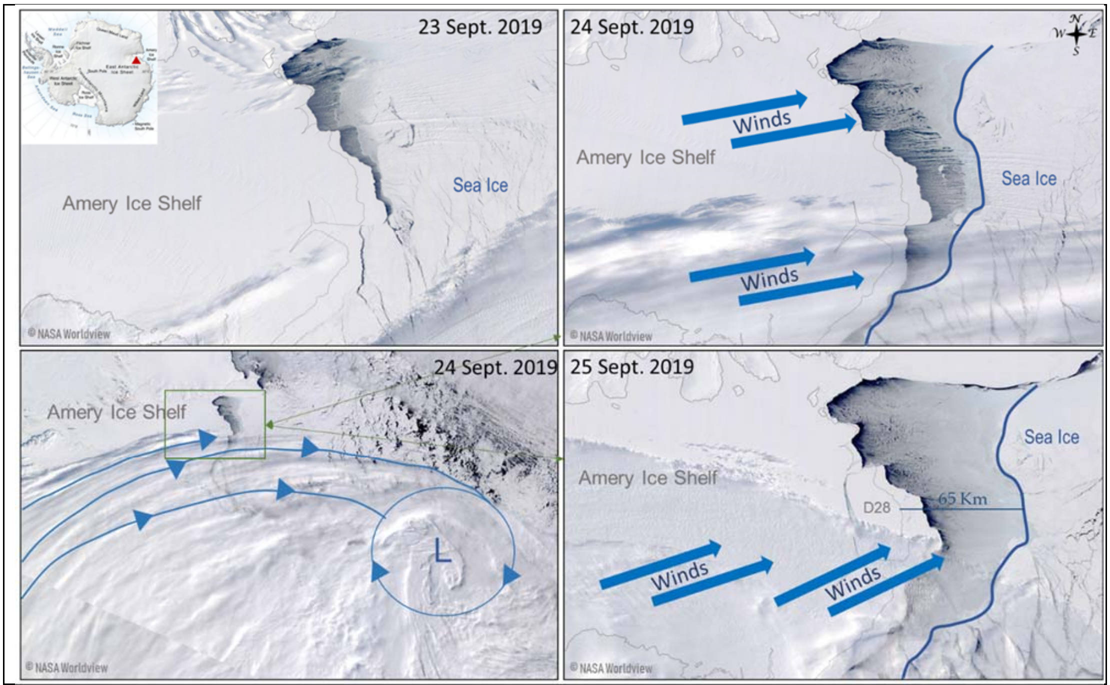

Figure 8: MODIS satellite visible imagery of the Amery Ice Shelf showing the ice shelf before the calving on 23 September 2019, during the calving on 24-25 September 2019. Image credit: NASA Worldview.

3. Discussion and conclusions

In this study, the role of atmospheric extremes in ice shelf instability is addressed by investigating the atmospheric conditions during the recent calving event from the Amery Ice Shelf on 25 September 2019. During the month of September 2019, the circulation around Antarctica was characterized by anomalously-pronounced 3 ridges and 3 troughs with the Indian sector of the Southern Ocean being under the influence of troughing and surrounded by two blocking ridges; one over the southern Atlantic to the west and one over Davis Sea and southern Australia to the east.

During the second half of September 2019, a series of explosive polar cyclones, evolving into stationary twin polar cyclones, impacted the region of the Amery Ice Shelf. The first explosive cyclone occurred on 18 September 2019 and evolved into two stationary twin polar cyclones on 19-22 September 2019 sitting to the west of the ice shelf. The second explosive cyclone formed on 23 September 2019 and evolved into two stationary twin polar cyclones on 24-25 September 2019, sitting, this time, to the east of the Amery Ice Shelf. Both explosive-cyclone episodes were accompanied by intense atmospheric rivers bringing anomalous warm and moist air masses poleward. The stationary aspect of the deep cyclones had a large impact on the ice conditions as it subjected the ice to sustained stress and strain. The main difference between the two episodes is the location at which the twin cyclones were stationary, relative to the Amery Ice Shelf, which

https://doi.org/10.5194/tc-2020-219
Preprint. Discussion started: 19 August 2020

The Cryosphere Discussions
Open Access
EGU

determined the characteristics of the air masses and the wind direction that affected the ice shelf. This position of the cyclones relative to the Amery Ice Shelf was, in turn, determined in each episode, by the location of the blocking ridges in the general circulation.

During the first episode, anomalous warm, moist and easterly winds impacted the ice shelf and surrounding sea ice, whereas during the second episode, the ice shelf and surrounding sea ice were under the influence of anomalous westerlies. The first episode resulted in a weakened and more exposed ice shelf due to (i) sea ice melting, and (ii) fracture amplification along the rift via wind-induced waves parallel to it. During the second episode, anomalously strong offshore winds resulted in an ice-free area in front of the western side of the ice shelf. Sustained strong winds perpendicular to the pre-existing rift induced (i) significant sea ice drift away from the shelf-front, (ii) sustained strain on the shelf-front, and (iii) fracture amplification along the rift leading to the calving. The detached iceberg after calving followed a northeasterly motion being dragged by the prevailing winds and associated ocean currents. This drifting direction was similar to the one followed by the sea ice one day before and gave an indication of the impact of the wind direction on this process. Given the east-exposed orientation of the crack at the ice shelf-front, the direction of the sustained strong westerly winds was deterministic for the calving.

In summary, atmospheric forcings by the explosive twin polar cyclones and associated atmospheric rivers, triggered the September 2019 breakoff at the Amery Ice Shelf via the interplay between several mechanisms:

- Thermodynamical processes linked to the poleward transport of anomalous warm and moist air masses which resulted in a reduction in sea ice concentration at the front of the ice shelf, thus increasing the exposure of the ice shelf-front to winds and waves.

- Mechanical forcing by the anomalously strong winds on: 1- Waves/swells which resulted in a cumulative shelf-front fatigue and amplification of the fractures along the pre-existing rift. 2- Sea ice drift which removed the protective buffer and increased the effect of wind-induced waves on the ice shelf margin. 3- The rift which led to the enlargement of the fracture and separated the iceberg from the shelf along the rift. 4- Subsurface warm waters which may have generated an influx of warm circumpolar deep water onto the ice shelf margin and under the ice shelf cavity that could have preconditioned the breakoff through basal melt (Morrison et al., 2020). The last point has not been explored in this study since it focuses on the role of atmospheric forcing on the calving.

The analysis of this unique event could help better understand the underlying factors leading to calving and ice shelf weakening; important precursors to ice shelf instability and disintegration and hence contribution to sea level rise. Our analysis highlights the need for ice sheet models, used to project sea level rise, to account for atmospheric forcing at high resolution, in addition to sea ice and ocean waves, if they were to simulate accurately the changes occurring in the ice sheet and glaciers and their contribution to sea level rise. Up till now, the role of warming ocean has been the focus of most of the scientific research on this topic, however, recent studies based on numerical experiments demonstrate that wind stress changes over the Southern Ocean drive enhanced poleward heat transport by stronger subpolar gyres and reduce coastal sea ice and cold-

https://doi.org/10.5194/tc-2020-219
Preprint. Discussion started: 19 August 2020

water formations, both of which result in an increased ocean heat flux into Antarctic ice shelf cavities (Kusahara, 2020). Furthermore, the increase of sea ice–free days can lead to enhanced regional subwater contribution to the basal melting.

In fact, important changes in the atmospheric circulation are being observed in the Southern Hemisphere. For instance, between 1979 and 2010 the subtropical jet streams moved poleward by 6.5 ± 0.2 degrees in the Southern Hemisphere (Hudson, 2012) and the westerlies strengthened and shifted poleward (Fogt and Marshal, 2020). The observed poleward movement over the past few decades represents a significant change in the position of the sub-tropical jet stream, which should lead to significant latitudinal shifts in the global weather patterns, the hydrological cycle and their impact on Antarctic ice shelves.

The variability of the polar jet front in the Southern Hemisphere and whether similar behavior as the polar jet in the Northern Hemisphere is underway around Antarctica needs to be investigated in future work. Several studies have shown evidence for a wavier jet stream in response to rapid Arctic warming and reported a weakening of the polar jet as a result of a reduced temperature gradient between high and mid-latitudes due to the increased temperatures in the Arctic (e.g., Francis and Vavrus, 2015; Coumou et al., 2015; Mann et al., 2017). Such change in the polar jet, which acts as an isolation boundary between high and mid latitudes, would lead to more interactions, and spark feedback mechanisms between the Antarctic system and mid-latitudes as it happened to be the case in the Arctic (Francis et al., 2018; 2019a).

The poleward shift of the cyclones together with the decrease in sea ice extent in recent years makes it more urgent to assess the impact of cyclones on Antarctic-wide maritime-terminating ice shelves as higher numbers of large cyclones could be expected to reach further south and therefore affects ice shelves dynamics. If extreme polar cyclones are to form or reach more frequently ice shelves due to climate change, their destructive effect may have important consequences and needs to be accounted for in models used for sea level and Antarctic Ice Sheet mass balance projections.

4. Data and methods

The atmospheric analysis is based on data from the ERA5 reanalysis (Hersbach et al., 2020). During the period 16-25 September 2019, hourly maps of mean sea level pressure (MSLP), winds, 2m temperature and total column water vapor (TCWV) are analyzed. Furthermore, in order to investigate the anomalous character of the atmospheric conditions, we calculated, for the same period and quantities listed above, hourly standardized anomalies and percentile ranks relative to all hourly ERA5 September values during the full record (1979-2019) over the area 45-95°E, 50-75°S. In addition, a histogram analysis has been performed over a smaller domain limited to the ice-shelf front area and adjacent mouth of Prydz Bay (i.e., 70-65°S and 70-75°E). The histograms represent the distribution of hourly values spatially averaged over this domain, for all months during 1979-2019.

Daily sea ice extent and concentration data are derived from the AMSR-E / AMSR2 unified record (Meier et al., 2018) at 12.5 km spatial resolution (https://nsidc.org/data/AU_SI12/versions/1). To check the motion in the sea ice field in the Amery Basin, we used the low-resolution sea ice drift product of the EUMETSAT Ocean and Sea Ice Satellite Application Facility (OSI SAF, www.osi-

https://doi.org/10.5194/tc-2020-219
Preprint. Discussion started: 19 August 2020

The Cryosphere Discussions
Open Access
EGU

saf.org). This is a 48-hour average gridded ice drift dataset processed on a daily basis and made available on a 62.5 km Polar Stereographic Grid (e.g., Kwok et al. 2017). Ice motion vectors are estimated by an advanced cross-correlation method on pairs of satellite images (Lavergne et al., 2010). It uses the multi-sensor spatial covering product that combines SSMIS (91 GHz H and V polarization) on board DMSP platform F17, ASCAT (C-band backscatter) on board EUMETSAT platform Metop-A, and AMSR-2 on board JAXA platform GCOM-W. Due to atmospheric noise and surface melting these data are only available for the Southern Hemisphere winter (1st April to 31st October).

Visible imagery of the Amery Ice Shelf and surrounding area are taken from MODIS/VIIRS land products (ORNL DAAC, 2018) using the NASA Worldview application (https://worldview.earthdata.nasa.gov).

Sentinel-1 data has been used to determine potential surface melt (e.g. Datta et. al, 2019) and to track ice velocity over the Amery ice shelf prior to the D28 iceberg calving by using feature tracking in ESA's SNAP Sentinel-1 toolbox. Sentinel-3A and 3B data were used via the ESA Ocean Virtual Laboratory application to determine the wave height at the front of the Amery Ice Shelf.

Acknowledgments

We acknowledge the use of imagery from the NASA Worldview application (https://worldview.earthdata.nasa.gov), part of the NASA Earth Observing System Data and Information System (EOSDIS). This work was supported by Masdar Abu Dhabi Future Energy Company, United Arab Emirates, Grant 8434000221. The contribution of Petra Heil was supported by the Australian Government's Australian Antarctic Partnership Program, and contributes to AAS Project 4506.

Code and Data availability: All data needed to evaluate the conclusions in the paper are present in the paper. Correspondence and requests for materials should be addressed to DF.

Author contributions D.F. conceived the study and wrote the initial manuscript. K.M. analyzed the satellite and reanalysis data. S.L analyzed satellite data. M.T. and P.H. provided input on result analysis. All authors interpreted results and provided input to the final manuscript.

Competing Interests The authors declare that they have no competing interests.

The Cryosphere Discussions

References

1. Allen, J.T., Pezza, A. B., and Black, M. T. (2010) Explosive cyclogenesis: a global climatology comparing multiple reanalyses. Journal of Climate, v.23, 6468–6484.
2. Aitken, A., Roberts, J., Ommen, T. et al. Repeated large-scale retreat and advance of Totten Glacier indicated by inland bed erosion. Nature 533, 385–389 (2016). https://doi.org/10.1038/nature17447.
3. Barnes, E. A., and L. Polvani (2013), Response of the midlatitude jets, and of their variability, to increased greenhouse gases in the CMIP5 Models, J. Clim., 26, 7117– 7135.
4. Bassis, J., Fricker, H., Coleman, R., & Minster, J. (2008). An investigation into the forces that drive ice-shelf rift propagation on the Amery Ice Shelf, East Antarctica. Journal of Glaciology, 54(184), 17-27. doi:10.3189/002214308784409116.
5. Bassis, J. N. and Ma, Y.: Evolution of basal crevasses links ice shelf stability to ocean forcing, Earth Planet. Sci. Lett., 409, 203–211, https://doi.org/10.1016/j.epsl.2014.11.003, 2015.
6. Bengtsson, L., K. I. Hodges, and N. Keenlyside (2009), Will extratropical storms intensify in a warmer climate? J. Clim., 22(9), 2276– 2301.
7. Benn D. I. and J. A. Åström (2018) Calving glaciers and ice shelves, Advances in Physics: X, 3:1, DOI: 10.1080/23746149.2018.1513819.
8. Bromirski, P. D., Sergienko, O. V. & MacAyeal, D. R. Transoceanic infragravity waves impacting Antarctic ice shelves. Geophys. Res. Lett. 37, L02502 (2010).
9. Chang, E. K. M., Y. Guo, and X. Xia (2012), CMIP5 multimodel ensemble projection of storm track change under global warming, J. Geophys. Res., 117, D23118, doi:10.1029/2012JD018578.
10. Chang, E. K. M., 2017: Projected Significant Increase in the Number of Extreme Extratropical Cyclones in the Southern Hemisphere. J. Climate, 30, 4915–4935, https://doi.org/10.1175/JCLI-D-16-0553.1.
11. Cook, A. J. and Vaughan, D. G.: Overview of areal changes of the ice shelves on the Antarctic Peninsula over the past 50 years, The Cryosphere, 4, 77–98, https://doi.org/10.5194/tc-4-77-2010, 2010.
12. Coumou D., J. Lehmann, J. Beckmann, (2015), The weakening summer circulation in the Northern Hemisphere mid-latitudes, Science, Vol. 348, Issue 6232, pp. 324-327. DOI: 10.1126/science.1261768.
13. Datta, R. T. Tedesco, M., Fettweis, X., Agosta, C., Lhermitte, S., Lenaerts, J.T.M., Wever, N. (2019) The Effect of Foehn-Induced Surface Melt on Firn Evolution Over the Northeast Antarctic Peninsula. Geophys. Res. Lett. 46, 3822–383, doi: 10.1029/2018GL080845.
14. Davies, H. C., 1997: Emergence of the mainstream cyclogenesis theories. Meteor. Z.,6, 261–274.
15. DeConto, R., Pollard, D. Contribution of Antarctica to past and future sea-level rise. Nature 531, 591–597 (2016), https://doi.org/10.1038/nature17145.
16. Dolatshah, A., Nelli, F., Alberello, A., Bruneau, L., Bennetts, L. G., Meylan, M. H., Monty, J. P., and Toffoli, A. "Wave Attenuation due to Ice Cover: An Experimental Model in a Wave-Ice Flume." Proceedings of the ASME 2017 36th International Conference on Ocean, Offshore and Arctic Engineering. Volume 8: Polar and Arctic Sciences and Technology; Petroleum

https://doi.org/10.5194/tc-2020-219
Preprint. Discussion started: 19 August 2020

The Cryosphere Discussions Open Access EGU

Technology. Trondheim, Norway. June 25–30, 2017. V008T07A016. ASME. https://doi.org/10.1115/OMAE2017-61548.

17. Eayrs, C., Holland, D. M., Francis, D., Wagner, T. J. W., Kumar, R., & Li, X. (2019). Understanding the seasonal cycle of Antarctic sea ice extent in the context of longer-term variability. Reviews of Geophysics. 57, 1037– 1064, https://doi.org/10.1029/2018RG000631.
18. Ferreira, R. N., W. N.Schubert, and J. J.Hack, 1996: Dynamical aspects of twin tropical cyclones associated with the Madden–Julian oscillation.J. Atmos. Sci., 53, 929–945.
19. Francis J. A. and S. J. Vavrus, 2015, Evidence for a wavier jet stream in response to rapid Arctic warming, Environ. Res. Lett. 10 014005.
20. Francis D., C. Eayrs, J-P. Chaboureau, T. Mote, D. Holland (2018), "Polar jet associated circulation triggered a Saharan cyclone and derived the poleward transport of the African dust generated by the cyclone" Journal of Geophysical Research: Atmospheres. DOI:10.1029/2018JD029095.
21. Francis D., C. Eayrs, J-P. Chaboureau, T. Mote, D. Holland (2019a), A meandering polar jet caused the development of a Saharan cyclone and the transport of dust toward Greenland, Adv. Sci. Res., 1, 1–8, https://doi.org/10.5194/asr-16-49-2019, 2019.
22. Francis D., C. Eayrs, J. Cuesta, D. Holland (2019b), Polar cyclones at the origin of the reoccurrence of the Maud Rise Polynya in austral winter 2017, Journal of Geophysical Research: Atmospheres,124. https://doi.org/10.1029/2019JD030618, 2019.
23. Francis D., K.S. Mattingly, N. Alshamsi, M. Temimi, R. Massom, P. Heil, 2020, On the crucial role of atmospheric rivers in the two major Weddell Polynya events in 1973 and 2017 in Antarctica. Sci. Adv. Under review.
24. Fricker, H., Young, N., Allison, I., & Coleman, R. (2002). Iceberg calving from the Amery Ice Shelf, East Antarctica. Annals of Glaciology, 34, 241-246. doi:10.3189/172756402781817581
25. Fricker, H. A., N. W. Young, R. Coleman, J. N. Bassis, and J.-B. Minster (2005), Multi-year monitoring of rift propagation on the Amery Ice Shelf, East Antarctica, Geophys. Res. Lett., 32, L02502, doi:10.1029/2004GL021036.
26. Fogt, RL, Marshall, GJ. The Southern Annular Mode: Variability, trends, and climate impacts across the Southern Hemisphere. WIREs Clim Change. 2020; 11:e652. https://doi.org/10.1002/wcc.652
27. Fyfe, J. C. (2003), Extratropical Southern Hemisphere cyclones: Harbingers of climate change?, J. Clim., 16, 2802– 2805.
28. Galton-Fenzi, B. K., J. R. Hunter, R. Coleman, S. J. Marsland, and R. C. Warner (2012), Modeling the basal meltingand marine ice accretion of the Amery Ice Shelf, J. Geophys. Res., 117, C09031, doi:10.1029/2012JC008214.
29. Greenbaum, J., Blankenship, D., Young, D. et al. Ocean access to a cavity beneath Totten Glacier in East Antarctica. Nature Geosci 8, 294–298 (2015). https://doi.org/10.1038/ngeo2388.
30. Grieger J., G. C. Leckebusch, C. C. Raible, I. Rudeva & I. Simmonds (2018) Subantarctic cyclones identified by 14 tracking methods, and their role for moisture transports into the continent, Tellus A: Dynamic Meteorology and Oceanography, 70:1, 1-18, DOI: 10.1080/16000870.2018.1454808.

https://doi.org/10.5194/tc-2020-219
Preprint. Discussion started: 19 August 2020

The Cryosphere Discussions
Open Access
EGU

31. Hersbach, H., Bell, B., Berrisford, et al., (2020), The ERA5 Global Reanalysis. Q J R Meteorol Soc. doi:10.1002/qj.3803.
32. Hogg, A., Gudmundsson, G. Impacts of the Larsen-C Ice Shelf calving event. Nature Clim Change 7, 540–542 (2017). https://doi.org/10.1038/nclimate3359.
33. Holdsworth, G. & Glynn, J. Iceberg calving from floating glaciers by a vibration mechanism. Nature 274, 464–466 (1978).
34. Hudson, R. D.: Measurements of the movement of the jet streams at mid-latitudes, in the Northern and Southern Hemispheres, 1979 to 2010, Atmos. Chem. Phys., 12, 7797–7808, https://doi.org/10.5194/acp-12-7797-2012, 2012.
35. Jeong, S., I. M. Howat, and J. N. Bassis (2016), Accelerated ice shelf rifting and retreat at Pine Island Glacier, WestAntarctica, Geophys. Res. Lett., 43,11,720–11,725, doi:10.1002/2016GL071360.
36. King, M. A., R. Coleman, A.-J. Freemantle, H. A. Fricker, R. S. Hurd, B. Legrésy, L. Padman, and R. Warner (2009), A 4-decade record of elevation change of the Amery Ice Shelf, East Antarctica, J. Geophys. Res., 114, F01010, doi:10.1029/2008JF001094.
37. Kohout, A., Williams, M., Dean, S. et al. Storm-induced sea-ice breakup and the implications for ice extent. Nature 509, 604–607 (2014). https://doi.org/10.1038/nature13262
38. Kossin P.J., K.R. Knapp, T.L. Olander, C.S. Velden, 2020, Global increase in major tropical cyclone exceedance probability over the past four decades, Proceedings of the National Academy of Sciences May 2020, 201920849; DOI: 10.1073/pnas.1920849117.
39. Kusahara, K., 2020: Interannual-to-Multidecadal Responses of Antarctic Ice Shelf–Ocean Interaction and Coastal Water Masses during the Twentieth Century and the Early Twenty-First Century to Dynamic and Thermodynamic Forcing. J. Climate, 33, 4941–4973, https://doi.org/10.1175/JCLI-D-19-0659.1.
40. Kwok, R., Pang, S. S., and Kacimi, S.: Sea ice drift in the Southern Ocean: Regional patterns, variability and trends, Elem. Sci. Anth., 5, 1–16, https://doi.org/10.1525/elementa.226, 2017.
41. Lambert, S. J., and J. C. Fyfe (2006), Changes in winter cyclone frequencies and strengths simulated in enhanced greenhouse warming experiments: Results from the models participating in the IPCC diagnostic exercise, Clim. Dyn., 26, 713– 728.
42. Lavergne, T., Eastwood, S., Teffah, Z., Schyberg, H., and Breivik, L.-A. (2010), Sea ice motion from low-resolution satellite sensors: An alternative method and its validation in the Arctic, J. Geophys. Res., 115, C10032, doi:10.1029/2009JC005958.
43. Lim, Eun-Pa; Simmonds, Ian (2002). Explosive Cyclone Development in the Southern Hemisphere and a Comparison with Northern Hemisphere Events. Monthly Weather Review. 130 (9): 2188–2209. Bibcode:2002 MWRv. .130.2188L. doi:10.1175/1520-0493(2002)130<2188:ECDITS>2.0.CO;2.
44. Liu Y., J. C. Moore, X. Cheng, R. M. Gladstone, J. N. Bassis, H. Liu, J. Wen, F. Hui, 2015, Iceberg calving of Antarctic ice shelves, Proceedings of the National Academy of Sciences, March 2015, 112 (11) 3263-3268; DOI: 10.1073/pnas.1415137112.
45. Mann, M., Rahmstorf, S., Kornhuber, K. et al. Influence of Anthropogenic Climate Change on Planetary Wave Resonance and Extreme Weather Events. Sci Rep 7, 45242 (2017). https://doi.org/10.1038/srep45242

https://doi.org/10.5194/tc-2020-219
Preprint. Discussion started: 19 August 2020

46. Massom, R.A., Scambos, T.A., Bennetts, L.G. et al. Antarctic ice shelf disintegration triggered by sea ice loss and ocean swell. Nature 558, 383–389 (2018). https://doi.org/10.1038/s41586-018-0212-1.
47. Matear, R., O'Kane, T., Risbey, J. et al. Sources of heterogeneous variability and trends in Antarctic sea-ice. Nat Commun 6, 8656 (2015). https://doi.org/10.1038/ncomms9656.
48. Meier, W. N., T. Markus, and J. C. Comiso. 2018. AMSR-E/AMSR2 Unified L3 Daily 12.5 km Brightness Temperatures, Sea Ice Concentration, Motion & Snow Depth Polar Grids, Version 1. [Antarctica]. Boulder, Colorado USA. NASA National Snow and Ice Data Center Distributed Active Archive Center. doi: https://doi.org/10.5067/RA1MIJOYPK3P [10 April 2020].
49. Morrison K.A., A. M. Hogg, M.H. England and P. Spence Warm Circumpolar Deep Water transport toward Antarctica driven by local dense water export in canyons, Science Advances, 2020: Vol. 6, no. 18, eaav2516, DOI: 10.1126/sciadv.aav2516.
50. Moustaoui, M., H. Teitelbaum, C. Basdevant, and Y. Boughaleb, Linked behavior of twin tropical cyclones, J. Geophys. Res., 107(D19), 4378, doi:10.1029/2000JD000066, 2002.
51. ORNL DAAC. 2018. MODIS and VIIRS Land Products Global Subsetting and Visualization Tool. ORNL DAAC, Oak Ridge, Tennessee, USA. Accessed May 20, 2020. Subset obtained for MOD13Q1 product over the Amery Ice Shelf – Antarctica, time period: 2019-09-01 to 2019-09-30. https://doi.org/10.3334/ORNLDAAC/1379.
52. Pope, J. O., Holland, P. R., Orr, A., Marshall, G. J., and Phillips, T. (2017), The impacts of El Niño on the observed sea ice budget of West Antarctica, Geophys. Res. Lett., 44, 6200– 6208, doi:10.1002/2017GL073414.
53. Pritchard, H. D., Ligtenberg S.R., Fricker H.A., Vaughan D.G., van den Broeke MR, Padman L., Antarctic ice-sheet loss driven by basal melting of ice shelves. Nature 484, 502–505 (2012).
54. Reale M., M. L.R. Liberato, P. Lionello, J. G. Pinto, S. Salon & S. Ulbrich (2019) A Global Climatology of Explosive Cyclones using a Multi-Tracking Approach, Tellus A: Dynamic Meteorology and Oceanography, 71:1, DOI: 10.1080/16000870.2019.1611340.
55. Raphael, M. N., 2007, The influence of atmospheric zonal wave three on Antarctic sea ice variability, J. Geophys. Res., 112, D12112, https://doi.org/10.1029/2006JD007852, 2007.
56. Renfrew A.I., G.W.K. Moore and A.A. Clerk (1997) Binary interactions between polar lows, Tellus A: Dynamic Meteorology and Oceanography, 49:5, 577-594, DOI: 10.3402/tellusa.v49i5.14823.
57. Rignot, E. et al. Accelerated ice discharge from the Antarctic Peninsula following the collapse of Larsen B ice shelf. Geophys. Res. Lett. 31, https://doi. org/10.1029/2004gl020697 (2004).
58. Rignot E., J. Mouginot, B. Scheuchl, M. van den Broeke, M. J. van Wessem, M. Morlighem, 2019, Four decades of Antarctic Ice Sheet mass balance from 1979–2017, Proceedings of the National Academy of Sciences Jan 2019, 116 (4) 1095-1103; DOI: 10.1073/pnas.1812883116.
59. Robinson, W. & Haskell, T. G. Calving of Erebus Glacier tongue. Nature 346, 615–616 (1990).
60. Robinson, W. & Haskell, T. G. Travelling flexural waves in the Erebus Glacier Tongue, McMurdo Sound, Antarctica. Cold Reg. Sci. Technol. 20, 289–293 (1992).
61. Sanders, Frederick; Gyakum, John R (1980). "Synoptic-Dynamic Climatology of the 'Bomb'". Monthly Weather Review. 108 (10): 1589–606. Bibcode:1980 MWRv.108.1589S. doi:10.1175/1520-0493(1980)108<1589:SDCOT>2.0.CO;2.

62. Scambos, T. A., Bohlander, J. A., Shuman, C. A. & Skvarca, P. Glacier acceleration and thinning after ice shelf collapse in the Larsen B embayment, Antarctica. Geophys. Res. Lett. 31,1 –4 (2004).
63. Schemm, S. (2018), Regional trends in weather systems help explain Antarctic sea ice trends. Geophysical Research Letters, 45, 7165–7175.https://doi.org/10.1029/2018GL079109.
64. Schlosser E., J.G. Powers, M.G. Duda, K.W. Manning (2011) Interaction between Antarctic sea ice and synoptic activity in the circumpolar trough: implications for ice-core interpretation, Annals of Glaciology 52(57) 2011.
65. Schlosser E., F. A. Haumann, M. N. Raphael Atmospheric influences on the anomalous 2016 Antarctic sea ice decay (2018), The Cryosphere, 12, 1103–1119, 2018, https://doi.org/10.5194/tc-12-1103-2018.
66. Schossler, V., Aquino, F.E., Reis, P.A. et al. Antarctic atmospheric circulation anomalies and explosive cyclogenesis in the spring of 2016. Theor Appl Climatol (2020). https://doi.org/10.1007/s00704-020-03200-9.
67. Shepherd, A., Fricker, H. A. & Farrell, S. L. Trends and connections across the Antarctic cryosphere. Nature 558, 223–232 (2018).
68. Shimada, U., A. Wada, K. Yamazaki, N. Kitabatake (2014) Roles of an upper-level cold vortex and low-level baroclinicity in the development of polar lows over the Sea of Japan, Tellus A: Dynamic Meteorology and Oceanography, 66:1, DOI: 10.3402/tellusa.v66.24694.
69. Smith, J.A., Graham, A.G.C., Post, A.L. et al. The marine geological imprint of Antarctic ice shelves. Nat Commun 10, 5635 (2019). https://doi.org/10.1038/s41467-019-13496-5.
70. Son, S.-W., L. M. Polvani, D. W. Waugh, H. Akiyoshi, R. Garcia, D. Kinnison, S. Pawson, E. Rozanov, T. G. Shepherd, and K. Shibata (2008), The impact of stratospheric ozone recovery on the Southern Hemisphere westerly jet, Science, 320, 1486– 1489.
71. Squire, V. A., Robinson, W. H., Meylan, M. H. & Haskell, T. G. Observations of flexural waves in the Erebus Glacier Tongue, McMurdo Sound, Antarctica, and nearby sea ice. J. Glaciol. 40, 377–385 (1994).
72. Stoll P.J., Graversen RG., Noer G, Hodges K. An objective global climatology of polar lows based on reanalysis data. QJRMeteorol.Soc.2018;144:2099–2117. https://doi.org/10.1002/qj.3309
73. Swart S., E. C. Cambell, C. H. Heuze, K. Johnson, J. L. Lieser, R. Masson, M. Mazloff, M. Meredith, P. Reid, J.-B. Sallee, S. Stammerjohn (2018) Litmus or sea ice anomaly? Sidebar, State of the Climate, BAMS, August 2018, DOI:10.1175/BAMS-D-18-0173.1.
74. Tamarin, T., and Y. Kaspi (2017), The poleward shift of storm tracks under global warming: A Lagrangian perspective, Geophys. Res. Lett., 44, 10,666–10,674, doi:10.1002/2017GL073633.
75. Turner J., S.A. Harangozo, G.J. Marshall, J.C. King, S.R. Colwell (2002) Anomalous atmospheric circulation over the Weddell Sea, Antarctica during the Austral summer of 2001/02 resulting in extreme sea ice conditions, Geophys.Res. Lett.,, Vol. 29, N0. 24, 2160, doi:10.1029/2002GL015565, 2002.
76. Uccellini L.W. (1990) Processes Contributing to the Rapid Development of Extratropical Cyclones. In: Newton C.W., Holopainen E.O. (eds) Extratropical Cyclones. American Meteorological Society, Boston, MA.

https://doi.org/10.5194/tc-2020-219
Preprint. Discussion started: 19 August 2020

77. Vaughan, D. G., H. F. J. Corr, R. A. Bindschadler, P. Dutrieux, G. H. Gudmundsson, A. Jenkins, T. Newman, P. Vornberger, and D. J. Wingham (2012), Subglacial melt channels and fracture in the floating part of Pine Island Glacier, Antarctica, J. Geophys. Res., 117, F03012, doi:10.1029/2012JF002360.
78. Vichi, M., Eayrs, C., Alberello, A., Bekker, A., Bennetts, L., Holland, D., et al. (2019). Effects of an explosive polar cyclone crossing the Antarctic marginal ice zone. Geophysical Research Letters, 46, 5948–5958. https://doi.org/ 10.1029/2019GL082457.
79. Wagner J.S., A. Gohm, A. Dörnbrack, A. Schäfler (2011), The mesoscale structure of a polar low: airborne lidar measurements and simulations. Q. J. R. Meteorol. Soc. DOI: 10.1002/qj.857.
80. Watanabe, S. I., and H. Niino, 2014: Genesis and Development Mechanisms of a Polar Mesocyclone over the Japan Sea. Mon. Wea. Rev., 142, 2248–2270, https://doi.org/10.1175/MWR-D-13-00226.1.
81. Wei, L., Qin, T. Characteristics of cyclone climatology and variability in the Southern Ocean. Acta Oceanol. Sin. 35, 59–67 (2016). https://doi.org/10.1007/s13131-016-0913-y.
82. Wille, J.D., V. Favier, A. Dufour, I. V. Gorodetskaya, J. Turner, C. Agosta, F. Codron (2019) West Antarctic surface melt triggered by atmospheric rivers, Nature Geoscience, https://doi.org/10.1038/s41561-019-0460-1.
83. Woods, C., and R. Caballero, 2016: The Role of Moist Intrusions in Winter Arctic Warming and Sea Ice Decline. J. Climate, 29, 4473–4485, https://doi.org/10.1175/JCLI-D-15-0773.1.
84. Yokoyama, Y.; Yamamoto, M., 2019, Influences of surface heat flux on twin cyclone structure during their explosive development over the East Asian marginal seas on 23 January 2008. Weather Clim. Extrem. 2019, 23, 100198. https://doi.org/10.1016/j.wace.2019.100198.
85. Zhao, C., Cheng, X., Liu, Y., Hui, F., Kang, J., Wang, X., Cheng, C. (2013). The slow-growing tooth of the Amery Ice Shelf from 2004 to 2012. Journal of Glaciology, 59(215), 592-596. doi:10.3189/2013JoG12J225.